

Coal Fly/Bottom Ash, Hydroxylapatite, and Hydrotalcite



Mudasir Mudasir, Roto Roto, Yoshinori Kuboki, and Parvin Begum

Contents

1	Coal Ash for the Adsorption of Dyes and Heavy Metal Ions in the Environments	462
1.1	Introduction to Coal Ash	462
1.2	Coal Bottom Ash (CBA)	463
1.3	Coal Fly Ash (CFA)	464
1.4	Acid Activation of Coal Ash	466
1.5	Modification of Coal Ash with Organic Ligand	467
1.6	Examples of Applications	470
1.7	Conclusion	473
2	New Functions of Hydroxyapatite in the Environmental and Medical Applications	474
2.1	Introduction	474
2.2	The Importance of Geometrical in the Scaffolds for Bone Reconstruction	476
2.3	Removal of Arsenate from Environmental Water by Hydroxyapatite Chromatographic System	483
2.4	Conclusion	489
3	Layered Double Hydroxides (LDHs) for Removal of Drug Trace in the Environment ...	489
3.1	Introduction to Layered Double Hydroxide (LDHs)	489
3.2	Syntheses of LDHs	491
3.3	Anion Exchange Properties of LDHs	493
3.4	Common Applications	494
4	Conclusion	498
	References	498

Abstract In this chapter, some inorganic materials such as coal ash, hydroxyapatite, and hydrotalcite are taken up as the adsorbents to remove pollutants in contaminated water and soil. Coal ash is a residual material that exists after all combustible

M. Mudasir (✉) and R. Roto
Faculty of Science, University of Gadjah Mada, Yogyakarta, Indonesia
e-mail: mudasir@ugm.ac.id; roto05@ugm.ac.id

Y. Kuboki and P. Begum
Faculty of Environmental Earth Science, Hokkaido University, Sapporo, Japan
e-mail: parvinchy@ees.hokudai.ac.jp

Shunitz Tanaka, Masaaki Kurasaki, Masaaki Morikawa, and Yuichi Kamiya (eds.), 461
Design of Materials and Technologies for Environmental Remediation,
Hdb Env Chem (2023) 115: 461–506, DOI 10.1007/698_2022_844,
© The Author(s), under exclusive license to Springer Nature Singapore Pte Ltd 2022,
Published online: 24 August 2022

material in coal has been burned. The main components of coal ash are silica (SiO_2) and alumina (Al_2O_3) and other metal oxides also exist. Although coal ash has some ability to adsorb pollutants, the ability increases by activation with acids and modification with an organic ligand like dithizone. The activated and modified coal ash were applied to the adsorption of cationic, anionic dyes and also Hg(II) . Hydroxyapatite (HAP), one form of Ca-phosphate compound, is a main component in bone as well as collagen. HAP is an important material biologically and it becomes an excellent adsorbent for arsenate. Firstly, our studies of HAP as the geometrical scaffolds for bone reconstruction are introduced and then the removal of arsenate from environmental water by HAP is discussed using a chromatographic system. Lastly, the adsorbing property of layered double hydroxides (LDHs), which are called hydrotalcite minerals, with the unique structure, is discussed as well as the synthesis methods.

Keywords Coal ash, Environmental applications, Hydrotalcite, Hydroxyapatite, Multifunctional materials

1 Coal Ash for the Adsorption of Dyes and Heavy Metal Ions in the Environments

1.1 Introduction to Coal Ash

Coal, as an energy source, in its combustion process produces several by-products. If the by-products are not used properly, it can cause environmental pollution. Based on the particle size, coal combustion ash is divided into two types, namely fly ash and bottom ash. The amount and characteristics of ash produced from coal combustion are determined by the type of coal and the combustion system used [1]. Coal ash is a residual material that exists after all combustible material in coal has been burned [2].

Based on energy use data, Indonesia uses a lot of energy sourced from coal. According to Oplas [3], the use of coal energy in Indonesia ranks first in ASEAN and tenth in the world. The rate of waste recycling of coal ash is not proportional to its production, hence it has the opportunity to cause pollution for the environment. Coal ash is a hazardous waste whose accumulation can trigger an explosion due to the formation of methane gas (CH_4). The accumulation of coal ash waste can also produce acid seepage which can damage soil fertility. To balance the rate of coal ash waste production, efforts are needed to utilize coal ash waste other than as a mixture of cement and construction materials [4].

The presence of silica (SiO_2) and alumina (Al_2O_3) content in ash allows coal ash to be used as an adsorbent. In its use as an adsorbent, fly ash is more common than bottom ash. This is because fly ash contains more silica and alumina, namely 56.13%

and 18.49%, while bottom ash is 50.98% and 14.99%, respectively. Production of fly ash waste is also higher, namely 80–90%, while bottom ash is 10–20% [5].

1.2 Coal Bottom Ash (CBA)

Coal ash is an amorphous adsorbent and comes from coal combustion. Coal burning produces coal bottom ash and fly ash by-products. Coal bottom ash is the ash left in the furnace. In Indonesia, the volume of this waste reaches 500–1,000 tons/day and is classified as hazardous waste. Coal bottom ash has a gray-black physical property and has a rougher surface than fly ash. The particle size of coal bottom ash is 10–100 μm .

The composition of coal ash depends on the type, source, application, and not the conditions of the kiln [6, 7]. Comparison of the compositions of coal bottom ash obtained from the coal burning at some Indonesian electricity power plants and sugar factory is presented in Table 1 [8–10]. Based on the table, bottom ash has the main components of silica and alumina. The presence of silica and alumina is the main reason why coal ash is used as an adsorbent. Silica present on the surface of the oxide particles is a weakly acidic silica monomer [11]. SiO_2 , CaO , Fe_2O_3 compounds can raise the pH, because metal oxides such as CaO can interact with water to form $\text{Ca}(\text{OH})_2$.

Some works have [12–14] reported that coal bottom ash has the main content of quartz and mullite. According to Murniati [15], characterization using XRD showed that the bottom ash was dominated by minerals quartz (SiO_2), mullite ($2\text{SiO}_2\cdot\text{Al}_2\text{O}_3$), and amorphous solids of silica and alumina. Other researchers [16, 17] have observed that coal ash before activation was amorphous, whereas

Table 1 Comparison of the composition of some coal bottom ash in Indonesia

Minerals	Percentage (% w/w)		
	PLTU paiton ^a [8]	PLTU IPMOMI ^a [9]	PG madukismo ^b [10]
Silica (SiO_2)	49.73	24.10	41.50
Alumina (Al_2O_3)	19.51	6.80	28.12
Iron oxide (Fe_2O_3)	16.18	33.59	15.37
Titania (TiO_2)	0.99	–	–
Magnesium oxide (MgO)	2.96	–	1.37
Calcium oxide (CaO)	5.40	26.30	1.25
Na_2O	1.23	–	4.25
K_2O	0.84	–	1.25
Mn_2O	0.17	0.32	–
Carbon (C)	–	11.50	–

Note: (–) not determined

^a Electricity power plant company

^b Sugar factory

after activation it was in the form of coarser (crystalline) deposits. Londar et al. [9] added that carbon inhibits crystal formation. Crystal formation is triggered by high temperatures, therefore carbon removal can be carried out through combustion (calcination). Ash with amorphous structure is more advantageous when used as a silica gel preparation material. The amorphous structure is easy to melt so as to produce optimal silica [18]. According to Padi [19], amorphous adsorbents have small pores so that their adsorption capacity is low.

An adsorbent with a high silica content is stable to high temperatures. Silica is resistant to temperatures up to 2,200°C. Coal fly ash and bottom ash have different levels of silica. Kula and Olgun [5] stated that coal fly ash contains more Si and Al than coal bottom ash. As a result, fly ash is more likely to be used as a geopolymer, cement additive, zeolite, and others. In the case of zeolites, Padi [19] found that the surface of the zeolite has oxide impurities that cover the pores and reduce absorption, so it must be activated first. NaOH and HCl can activate the adsorbent. According to Padi [19] and Mufrodi et al. [20], reflux using HCl solvent aims to enlarge pores, reduce impurities, partially dissolve alumina, and deionize Na metal. Other researchers [8, 17, 21] have used NaOH in the manufacture of zeolites. Smelting with NaOH aims to activate silica and alumina into soluble minerals. Sodium silica is soluble in water, while sodium alumina is soluble in alkali. NaOH can also expel silica and alumina from inside of the framework to the surface silica and alumina. Based on this result, coal bottom ash also has been treated and activated in the same manner as zeolite to remove oxide impurities.

The preparation of adsorbent from coal bottom ash has been studied by several researchers. Sunarti [8] has synthesized zeolite from coal bottom ash by smelting with NaOH and hydrothermal reaction. XRD data showed that smelting with NaOH produced amorphous silica and alumina and the adsorption study showed that the synthetic zeolite from bottom ash adsorbed more Pb(II) than the original bottom ash. The synthetic zeolite prepared from coal bottom ash is able to adsorb 99.74% Zn (II) [21]. The same adsorbent, e.g. synthetic zeolite prepared from coal bottom ash, is also able to adsorb Cu(II) with an adsorption capacity of 25 mg/g and the adsorption takes place chemically by involving the active site of the synthetic zeolite [15].

1.3 Coal Fly Ash (CFA)

Fly ash is a by-product of coal combustion which accounts for about 60–88% of the total coal combustion residue. Globally, its annual production is estimated at 0.75–1 billion tons. So far, fly ash is generally used as a mixture of concrete and road or dam construction [22]. The release of fly ash into the atmosphere is very dangerous for health if it is inhaled directly because fly ash is a particulate material that can affect DNA repair mechanisms through the formation of reactive organic species [23]. Currently, many studies use fly ash as a coagulant, catalyst, membrane filtration, photocatalysis, and the Fenton process [24].

Coal fly ash consists of a complex mixture of organic (1–9%) and inorganic (90–99%) constituents of which it is about 30–84% amorphous and 17–63% crystalline which is between 1 and 500 μm in size and has a particle size distribution of tri-modal which is mostly located below 75 μm . The color of coal fly ash depends on the unburnt carbon and iron content, it can be reddish brown due to iron or gray to black due to carbon content. The different components of coal fly ash induce the different structures or shapes, which are different from the aluminosilicate glass phase which is spherical, while in the crystalline phase quartz and unburned carbon are irregularly shaped particles [25]. The density of coal fly ash ranges from 0.54 to 0.86 g/cm^3 [22] and the surface area usually lies between 0.2 and 10 m^2/g , coal fly ash with unburned carbon content has a surface area of approx. 200 m^2/g [26].

Coal fly ash has properties such as particle size distribution, surface area, hydrophilicity, and porosity that are complex according to their origin and composition [27]. The main constituents of coal fly ash are silica, alumina, iron oxide, calcium oxide, and varying amounts of carbon [28]. Coal fly ash has an irregular structure (amorphous) above 90%. More than 80% of the inorganic composition consists of Al_2O_3 , SiO_2 , and Fe_2O_3 . Coal fly ash also contains small amounts of transition metal oxides which are active components of many catalytic systems such as Mn, Cr, Co, Ni, Zn, Cu [29, 30] (Table 2).

The classification of coal fly ash is based on the CaO content. If chemical elements such as silica, iron oxide, and alumina make up more than 70% of all raw ash, then it is categorized as F-type ash according to American Society for Testing and Materials (ASTM) C 618. If the content of silica, iron oxide, and alumina is <70% of the total raw ash, fly ash is categorized as C-type ash [31]. Another criterion according to the ASTM standard is that fly ash obtained from burning bituminous or anthracite coal is classified as Class-F and that obtained from burning subbituminous coal or lignite is classified as Class-C fly ash [32]. Most of the F-type coal fly ash have been used by researchers for water treatment applications and very few studies have used C-type fly ash [33].

Coal fly ash can be used as a gas adsorbent such as CO_2 [25], SO_2 , NO_x [34], and H_2S , because it has a high alkali content, namely calcium which is usually used as an adsorbent for acid gas in the process of controlling air pollution [35]. Coal fly ash can also be used for adsorption of dyes such as reactive black-5 (RB5) azo dye [36], methyl orange [37], acid blue-113 and tartrazine [38], indigo carmine and acid orange-52 [39], active red X-3B [40]. The adsorption of anthraquinone-dye (acid blue-127) and acid yellow-17 must be carried out at a pH lower than the pK_a of the dye, in order to form a stable cationic site so that adsorption can take place optimally [41].

Single or simultaneous adsorption of heavy metals with coal fly ash has been widely carried out. Metal adsorption is generally carried out with a batch system so that the adsorption runs optimally [42]. Before being used, the adsorbent is usually activated first to make it more effective. Activation can be done physically by heating or chemically by extracting coal fly ash with acids such as HCl [43] and base NaOH [44]. The purpose of activation is to enlarge the pores and remove

Table 2 Metal oxide compositions of Coal fly ash from PT Petrokimia Gresik, Indonesia [30]

No.	Metal oxides	Chemical composition (% w/w)
1.	SiO ₂	36.10
2.	Al ₂ O ₃	19.80
3.	Fe ₂ O ₃	24.1
4.	CaO	9.18
5.	MgO	–
6.	P ₂ O ₅	1.10
7.	SO ₃	0.40
8.	K ₂ O	1.27
9.	TiO ₂	1.88
10.	V ₂ O ₅	0.07
11.	Cr ₂ O ₃	0.03
12.	MnO	0.20
13.	ZnO	0.07
14.	MoO ₃	5.10
15.	BaO	0.30

impurity of metal oxides in coal fly ash so that the adsorption ability becomes better [27].

1.4 Acid Activation of Coal Ash

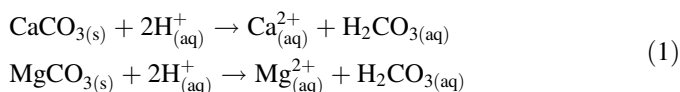
The existence of impurities in coal bottom ash including metal salts such as CaCO₃, MgCO₃, Fe₂S, and FeS and free heavy metals causes the ability of coal bottom ash for pollutants such as heavy metals and dyes to become less optimal, and therefore its adsorption capacity toward a certain pollutants is low [45]. In addition, if the impurities are not removed from the adsorbent, the presence of heavy metals in coal bottom ash can pollute the environment when coal ash is used as an adsorbent on a large scale. Therefore, it is necessary to do a treatment to remove impurities in the coal bottom ash. Various methods have been used to remove metal oxides from aluminasilica materials. One of them is activation with strong acids such as HCl, HNO₃, and H₂SO₄ [46].

Activation with strong acids usually has a strong influence on the structure and properties of the material because of the chemical interactions that occur between the strong acid and the surface of the material or adsorbent [47]. This method increases the adsorptive properties or adsorption capacity of coal ash by producing a more specific surface [45]. Inorganic acids or mineral acids such as HCl, H₂SO₄, HNO₃ are more commonly used in the activation process because they have a more significant effect than organic acids such as acetic, formic, oxalic acids [48]. Wang et al. [49] have reported that most of the metal oxides contained in coal ash dissolve in low pH. The dissolution intensity of metal oxides increases as the pH of the solution decreases. When coal ash is activated by strong inorganic acids like HCl,

Table 3 Analytical results of major components of coal fly ash from PT. Petrokimia Gresik before and after activation using AAS

Components	Coal fly ash before acid activation	Coal fly ash after acid activation
	Content (% w/w)	Content (% w/w)
SiO ₂	33.3	41.7
Al ₂ O ₃	16.0	17.0
CaO	0.57	0.38
Fe ₂ O ₃	12.7	4.87

the content of other minerals (metal oxides) except silica minerals will interact with the acid, then dissolve and cause the active site in the coal ash to be more open. This causes the active site of the adsorbent to become more accessible so that the adsorption capacity of coal ash increases [45]. An example of the dissolution reaction of metal oxides with strong acids is shown as Eq. (1) (Table 3).



1.5 Modification of Coal Ash with Organic Ligand

Dithizone is an organic ligand which is commonly used in spectrometric analysis and metal extraction. The chemical properties of dithizone are having the molecular formula C₁₃H₁₂N₄S, molecular weight 256.32 g/mol, boiling point 168°C, unstable to heat, non-polar at pH < 7, and when dissolved it produces a green solution. Dithizone is soluble in non-polar solvents such as ethanol, tetrachloride, chloroform, and benzene. Figure 1 shows the structure of dithizone in the keto and enol forms. According to Suseno [50], in the keto form, metal ions interact with -NH and in the enol form interact with -SH.

Dithizone is a ligand that can form coordinate covalent bonds with metal ions, through one or more of its donor atoms. Based on the number of donor atoms owned, ligands are grouped into monodentate, bidentate, and so on. Some complexes form weak ligand-metal bonds, so they decompose when dissolved in water. Metal ions that can form metal complexes with dithizone include Ag, Au, Bi, Cd, Co, Cu, Fe, Hg, Ni, Pb, Pd, Te, and Zn. The complex formed is generally neutral so that it can be extracted into the organic phase. According to Kunarti [51], ligands experience deprotonation at alkaline pH, so that their surface is negatively charged. The large number of OH⁻ ions causes competition between the OH⁻ ions in the solvent and the ligands. Under increasingly acidic conditions, the metal-dithizone complex becomes less stable. Meanwhile, under more alkaline conditions, the dithizonate complex was more stable. The gradual addition of ligands causes complex formation

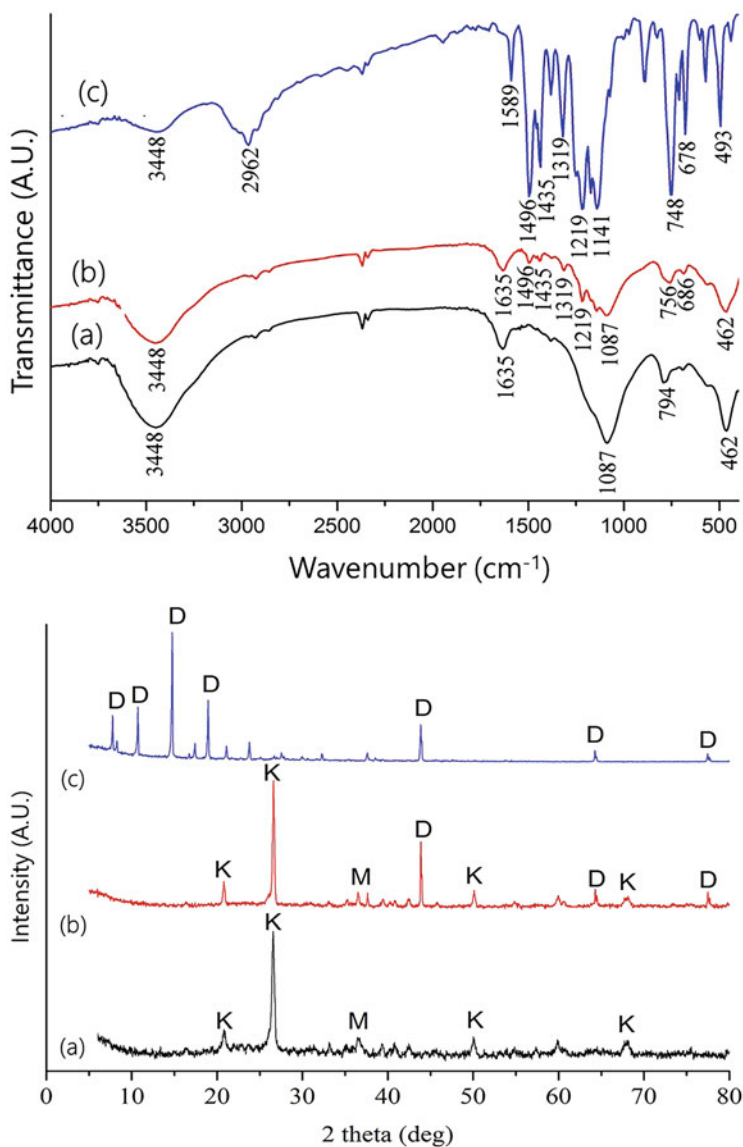


Fig. 1 Chemical structure of dithizone, showing keto and enol forms

to occur gradually. If there is excess ligand, the equilibrium reaction for complex formation shifts toward the product.

Because it has many donor atoms, dithizone can bind to both metal ions and solid supports. The most effective technique for binding dithizone to a solid support is through immobilization. Another technique that is often used is impregnation [18],

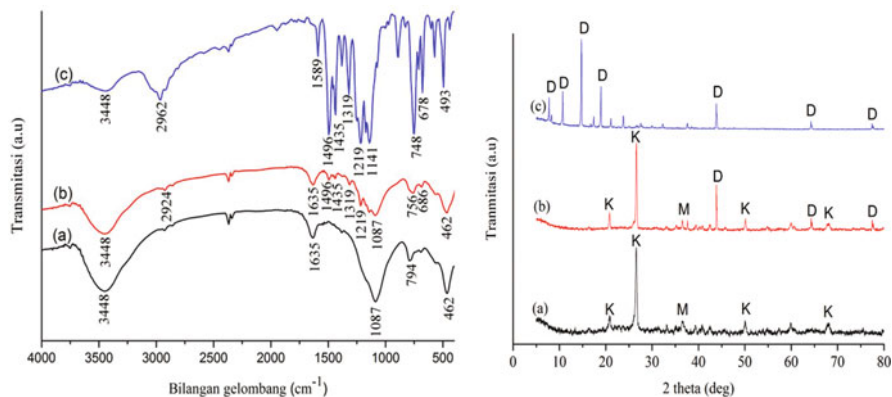


Fig. 2 Typical FTIR Spectra (left) and XRD pattern of Act-CBA (a), Dtz-CBA (b) and free dithizone (c)

but it is less effective because the interaction between the adsorbent and dithizone is less strong. Wogo et al. [52] stated that the modification of dithizone did not change the silica crystallization, but the surface area was reduced. Dithizone-immobilized silica gel shows a color change from gray to brick red, the more dithizone, the darker the color [53]. Several other researchers reported that dithizone can bind to poly EGDMA-co-HEMA (ethylene glycol dimethacrylate and 2-hydroxyethyl methacrylate), silica gel, chitin, natural zeolites, and others. Salih, et al. [54] reported that the order of single metal adsorption on dithizone-poly EGDMA-co-HEMA beads was $Pb(II) > Cr(II) > Hg(II) > Cd(II)$.

Several dithizone immobilization methods have been used by previous researchers. Salih et al. [54] carried out the immobilization of dithizone on poly EGDMA-co-HEMA by refluxing 0.5 g of dithizone, 3 g of polymer, and 4 g of NaOH. Reflux was carried out for 24 h, at a speed of 400 rpm and a temperature of 80°C. Another procedure was carried out by Absalan and Goudi [55], namely mixing 10 mL of dithizone with 40 mL of a suspension containing 1.5 g of alumina. The adsorbent is then used to adsorb Ag(I). Dithizone immobilized triacetylcellulosic membranes were prepared by Savafi and Bagheri [56] and used to adsorb Hg(II). The researchers also designed the same adsorbent to adsorb Cu (II) [57]. Immobilization of dithizone on chitin from shrimp shells has also been carried out by refluxing 4 g of biopolymer with 1 g of dithizone at 70°C. Reflux was carried out for 6 h and the adsorbent was used to adsorb Cd(II) [58]. The optimum adsorption of Cd(II) occurred at pH 6 with an adsorption capacity of 5.67 mol/g.

Silica-dithizone adsorbent was also prepared by refluxing 20 mL of silica suspension with 5 g of dithizone. Reflux was carried out for 24 h, then the adsorbent was used to study the kinetics and equilibrium of Hg(II) [53]. Yu et al. [59] have used dithizone immobilized silica gel to adsorb Cu(II). Silica gel activation was carried out by refluxing 20 g of silica gel with 10 mL of 6 M HCl for 5 h. The solids were washed to neutral and dried. The mixture was stirred for 48 h in 30 mL of dithizone

solution. The solid was washed with toluene, ethanol, water, then dried. Dithizone immobilized chitin for Cu(II) adsorption has also been reported [60].

Based on these various methods, in our study on the modification of coal ash, we have modified the previously reported method [19, 20, 59], which first used HCl to activate coal ash and then the activated adsorbent was modified with dithizone by immobilization. As reported by Jundu [18], immobilization with organic ligands is an effective way to get a higher adsorption capacity. The adsorbent modified with dithizone showed higher selectivity and capacity for heavy metals [58, 61–63]. Figure 2 gives the examples of typical FTIR spectra and XRD pattern of (a) activated coal bottom ash (Act-CBA), (b) dithizone-immobilized CBA (Dtz-CBA), and (c) free dithizone.

1.6 Examples of Applications

1.6.1 Adsorption of Cationic and Anionic Dyes

We have studied the adsorption of anionic dyes of coomassie brilliant blue (CBB) and cationic malachite green (MG) dyes using activated coal bottom ash (Act-CBA) as well as non-activated coal bottom ash (CBA). Coal bottom ash was activated by acid method by refluxing it in hydrochloric acid (HCl) for 4 h. Adsorption processes were conducted in batch method and some parameters influencing the adsorption performance were examined, including the effects of pH, adsorbent mass, contact time, and initial concentration of adsorbate. From this data then the kinetic models and isotherm adsorption were evaluated, and the example of dyes removal from synthetic samples containing both CBB or MG using Act-CBA was also carried out.

As expected the optimum removal of anionic CBB from solution of 50 mL, 20 ppm CBB using both CBA and Act-CBA is obtained at acidic solution of pH 3–4 because at this condition the surface of the adsorbent is positively charged (PZC of CBA = 5–6) [63], the optimum adsorbent mass is 0.3 g with the contact time of 90 min and initial dye concentration of 125 ppm. In contrast, the optimum adsorption of cationic MG from 50 mL, 40 ppm solution using either CBA or Act-CBA is obtained at alkaline pH of 8 with 0.2 g of adsorbent mass, 90 min of contact time; and 125 ppm of initial MG dye concentration. This is also easily understood as the surface of CBA will have negative net-charge at pH > 6. Effect of pH on the adsorption of dyes is given in Fig. 3. From the figure, it is obviously observed that Act-CBA adsorbs dyes more efficiently than the non-activated CBA. This is probably due to the dissolution of some metal oxide impurities that cover the active sites of the adsorbents.

The adsorption kinetics and isotherms were also studied in this research. The adsorption of the dyes by Act-CBA and CBA is best described by pseudo-second order kinetic models with the rate constants (k_2) for anionic CBB are 9.91×10^{-2} and 2.16×10^{-2} g/mg.min, respectively, and those for cationic MG are 2.16×10^{-2} and 1.52×10^{-2} g/mg.min, respectively. Isotherm adsorption studies indicate that

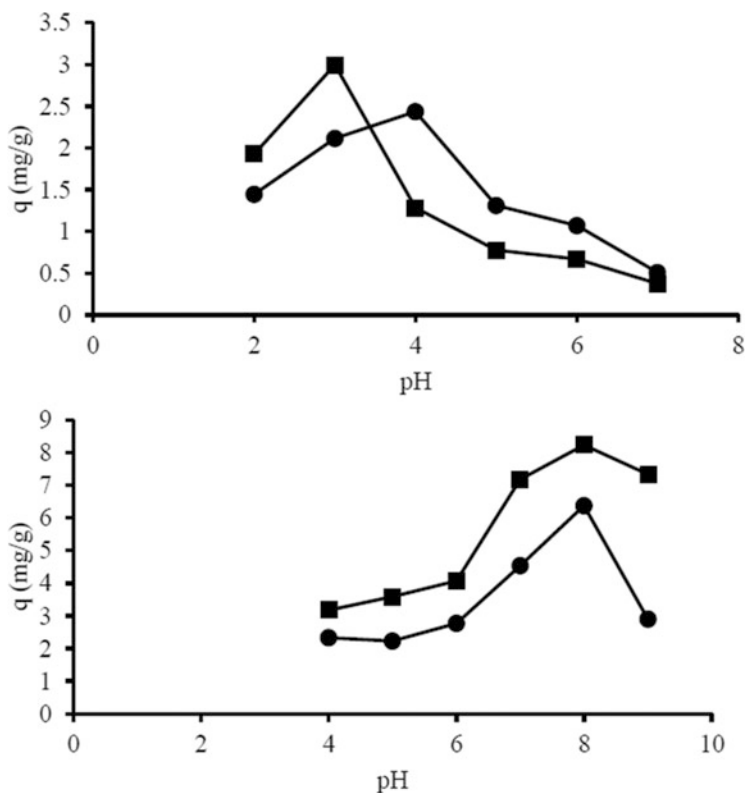


Fig. 3 Effect of pH on the adsorption capacity of CBB (upper) and MG (lower) dyes on CBA (circle) and Act-CBA (square)

Freundlich isotherm model best fits the adsorption of CBB with the Freundlich constants (K_F) for Act-CBA and CBA are respectively 5.54×10^{-4} and 2.73×10^{-4} mol/g. Meanwhile, the adsorption of cationic MG fits Langmuir isotherm model with the adsorption capacity (q_m) for Act-CBA and CBA are 1.98×10^{-5} and 6.63×10^{-5} mol/g, indicating the significant effect of acid activation on adsorption capacity of the adsorbent.

The adsorbent application for the adsorption of CBB and MG dyes in synthetic samples is shown in Fig. 4. From this figure, it can be seen that the concentration of coomassie brilliant blue dye decreased from 198.5 to 7.8 mg/L after five adsorption processes using HCl-activated coal bottom ash. The concentration of coomassie brilliant blue dye continuously decreased after the repetition of the adsorption process, which was 143.4; 97.2; 51.2; 20.9; and 7.8 mg/L, respectively. The adsorption percentage of the 1-fifth consecutive adsorption process also increased, namely 27.7; 51.0; 74.2; 89.4; and 96.1%, respectively. Figure 4 shows that the concentration of malachite green dye also decreased from 199.1 to 6.1 mg/L after three consecutive adsorption processes using HCl-activated coal bottom ash. The

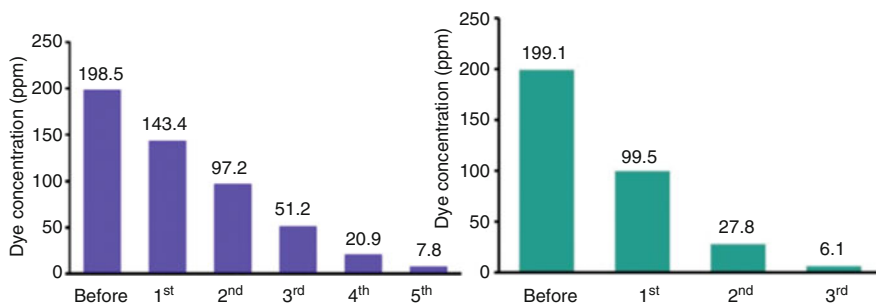


Fig. 4 Consecutive adsorption of MBB (left) and MG (right) from synthetic samples using Act-CBA at their optimum condition

decrease in the concentration of malachite green dye after the first to third adsorption process was 99.5; 27.8; and 6.1 mg/L, respectively, while the adsorption percent increased by 50.0; 86.0; and 96.9%. From these results, it is evident that coal bottom ash after activation can be used for the adsorption of cationic and anionic dyes by adjusting the pH of the solution.

1.6.2 Adsorption of Metal Ions

Many applications of coal ash for the adsorption of metal ions have been reported [58, 61–64]. Here we give one example of the application of coal bottom ash after being immobilized with dithizone (Dtz-CBA) for the adsorption of Hg(II) ions. The immobilization of dithizone was conducted in toluene medium, and the products were confirmed by some analytical methods [58, 61, 62]. The aims of dithizone immobilization is to increase adsorption selectivity and capacity of CBA toward Hg(II) ion. The parameters influencing the adsorption performance of Dtz-CBA and CBA toward Hg(II) ion such as pH solution, adsorbent mass, interaction time, and initial concentration (Fig. 5) were systematically optimized.

Results of our study have shown that the morphology of coal bottom ash characterized by SEM-EDS shows spherical and irregular shapes. The CBA contains mainly SiO₂ and Al₂O₃. FTIR spectra of Dtz-CBA show new peaks at 1,319 and 1,489 cm⁻¹ which are characteristics for –NH stretching and –CN bending of dithizone. XRD data shows basal spacing (d) at 4.28, 3.36, 3.72 Å for Dtz-CBA, while CBA shows basal spacing at 4.25, 3.69, 3.34 Å, indicating that both adsorbents are dominated by quartz and mullite minerals. GSA analysis shows the CBA surface area, pore volume, and pore radius were, respectively, 126.66 m²/g, 15.22 Å, and 0.10 mL/g and Dtz-CBA gives 13.48 m²/g, 17.02 Å, and 0.05 mL/g, respectively.

Adsorption study shows that Hg(II) is adsorbed chemically, and fitted well pseudo-second order kinetic models, and Freundlich isotherm models. At optimum condition the adsorption of Hg(II) on CBA is 68.958% using the initial concentration

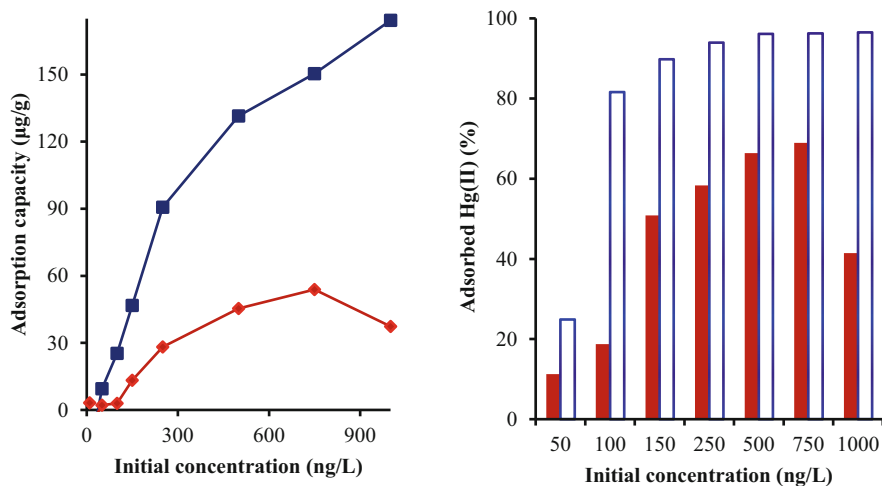


Fig. 5 Effect of initial concentration of Hg(II) on the adsorption performance of CBA (red) and Dtz-CBA

Table 4 Equilibrium constants (K), adsorption capacity (Q), and adsorption energy (E) for the adsorption of Hg(II) ion on coal bottom ash (CBA) and Dithizone-CBA (Dtz-CBA)

Adsorbents	R^2	K (L/mol)	Q (mol/g)	E (kJ/mol)
CBA	0.930	22,872.27	2.685×10^{-7}	24.869
Dtz-CBA	0.999	212×10^5	8.685×10^{-7}	41.795

of Hg(II) 750 ppb, and that of Dtz-CBA reaches 96.531% using the initial concentration of Hg(II) 1,000 ng/L. The adsorption capacity (Q), equilibrium constant (K), adsorption energy (E) (Table 4), and adsorption rate (k) for Hg(II) on Dtz-CBA are much higher than those on CBA, suggesting the effectiveness of dithizone immobilization in enhancing the adsorption ability of CBA. This is most probably due to the fact that Dtz-CBA has larger pore radius, and much more donating atom originating from dithizone so that the complexation between metal ion and active site of adsorbent is readily facilitated. These results have clearly proved that immobilization of specific organic ligand on the surface of certain adsorbents is able to increase the adsorption capacity of the adsorbents toward certain metal ions.

1.7 Conclusion

It has been shown that coal fly/bottom ash contains mainly silica and mullite minerals which are potential to be used as adsorbent for pollutants. Coal fly/bottom ash also contains impurities of metal oxides such as calcium and iron oxides. Acid activation of the coal fly/bottom ash before it is being used as adsorbent has proved

to be very effective and efficient methods to remove impurities of metal oxides that cover the surface of the adsorbents, so that their adsorption capacity toward either cationic or anionic dyes is significantly improved. Moreover, modification of the surface of coal fly/bottom ash with organic ligands such as dithizone has also increased the adsorption selectivity and capacity of the adsorbents to the heavy metal ions. In case of Hg(II) ion, it has been demonstrated that the adsorption capacity of dithizone-immobilized coal bottom ash is more three times higher than that of unmodified coal bottom ash. These results clearly demonstrated that coal fly/bottom ash can potentially be used for the adsorption of cationic and anionic dyes by adjusting the pH of the solution and that the modification of coal fly/bottom ash with specific organic ligand can be used as suitable strategy in enhancing the selectivity and capacity of coal fly/bottom ash toward heavy metal ions.

Acknowledgements The first author (M.M.) would like to acknowledge the partial financial support from Directorate General of Higher Education (DGHE), The Republic of Indonesia through research grants of Penelitian Dasar (PD), and Penelitian Dasar Unggulan Perguruan Tinggi (PDUPT) for fiscal year of 2021.

2 New Functions of Hydroxyapatite in the Environmental and Medical Applications

2.1 Introduction

Hydroxyapatite and collagen, as we see in this section, are the two main components of bone that exist as an exquisite molecular hybrid structure. Let us look at hydroxyapatite from the viewpoint of animal evolution. Mother Nature selected this mineral as the main component of bone about 0.4 billion years ago, in the Ordovician period. Surprisingly, there is one exception. In the Cambrian period, about 0.2 billion years before the appearance of HAP as a bone component, a brachiopod named *Lingulidae* equipped hydroxyapatite as a component of their exoskeleton, and they are still living only in Ariake Bay, Japan [65, 66]. From the above historical facts, we conceive that hydroxyapatite should be discussed with collagen as the extracellular matrices to understand the actual function. Therefore, this article will first discuss the latest medical application of hydroxyapatite to reconstruct bone tissue. Then, we will describe our new findings that hydroxyapatite: a component of bone, can remove the toxin (As) from environmental water.

What is hydroxyapatite?

To answer this question, we attempted a kind of decalogue for hydroxyapatite, by which we hope to give a glance at this exciting mineral.

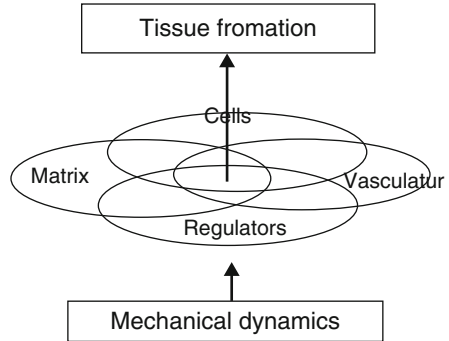
1. Hydroxyapatite (HAP) is one form of Ca-phosphate compound made of the 18 atomic groups, named by Werner, after the Greek word $\alpha\pi\alpha\tau\alpha\omega$ meaning “to deceive,” because of difficulty to distinguish from other minerals [67].

2. HAP is chemically and thermodynamically the most stable form among the many Ca-phosphate compounds, being highly insoluble in water but readily soluble in aqueous solvents at pH below 5.5 and can be used as a Ca-nutrient.
3. The unit cell of HAP crystal is composed of 18 atomic groups: $\text{Ca}_{10}(\text{PO}_4)_6(\text{OH})_2$, with the lattice: $a = 9.43 \text{ \AA}$, $c = 6.888 \text{ \AA}$, rhombic shape in ab-plane, rectangle in ac-plane.
4. HAP and collagen constitute the two main components of bone invertebrates, and both substances exist in bone tissue as the systematic hybrid at the nano-meter level [68].
5. HAP possesses strong adsorbing abilities for many minerals and organic compounds. The primary application of this property is for chromatography. Biochemically, HAP possesses a higher affinity for double chain DNA than the single one. This critical fact may suggest the involvement of HAP in animal evolution. (A hypothesis in this article.)
6. Adsorbing ability of HAP helps us to remove various harmful substances from the environment. One of the valuable medical applications is the preventive methods for athlete's foot [69].
7. HAP can be sintered to fine solid-state ceramics, which is highly valuable for orthopedic and dental fields. Aoki et al. developed this method (1972) [70]. Also, a traditional beautiful ceramics called "bone china" has probably contained HAP.
8. HAP is highly useful for bone reconstruction and cell substrates for cell culture: the powerful tool regenerative medicine.
9. The powders of pure HAP were shown to invest the micro defects on the surface of tooth enamel, thus believed to prevent the early development of tooth decay (micro-investing theory by Kuboki et al. 1972) [71, 72].
10. From the calcium resource of scallop shell composed of CaCO_3 , Kuboki et al. synthesized HAP in a recycled manner, performed HAP chromatography, and produced a HAP toothpaste [73].

For the past 60 years, our research group has engaged in the biochemistry of the hard tissues: bone and teeth. We had tried to clarify the mechanism of hard tissues (bone and teeth) formation and developed new technologies to reconstruct these tissues when they were disturbed. We concluded that the five factors must be considered: they are (1) cells, (2) extracellular matrices (ECM), (3) activating factors, (4) nutrition by vascularization, and (5) mechano-dynamic factors as illustrated in Fig. 6. For successful results in regenerative medicine, in our proposal, we must combine these five factors properly to lead the growth and differentiation of cells into specific active tissues and organs.

We have proposed that we consider five factors for the successful reconstruction of local tissues. These are (1) cells directly involved in tissue formation, (2) natural extracellular matrices (ECM) produced by the cells, or artificial ECM, (3) nutrition, provided by vascularization, (4) regulators for cellular activities, and (5) mechano-dynamic factors.

Fig. 6 Five factors that influence tissue formation and reconstruction



Among five factors, the cell is the primary importance, and the stem is the almighty cell that can create all kinds of tissues and organs. However, stem cell alone creates any tissue or organ. The stem cells first need their matrices. The matrices include natural and artificial HAP; the latter is often called a scaffold. Also, the cells need regulators, such as cytokines and vasculature, to supply nutrients, and people have often forgotten the mechano-dynamic factors. Still, we quickly understand if we imagine in utero situations [74].

This article concentrates on the matrix since HAP is one of the most valuable materials in constructing artificial ECM for bone reconstruction.






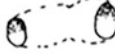
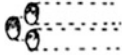




We have already pointed out that there are four fundamental requisites for the artificial ECM (scaffold), (1) physical, (2) chemical, (3) biochemical, and (4) geometrical properties [74, 75]. Because of the former three properties we see in all references in regenerative medicine, we will pay attention to the geometrical property hereafter.

2.2 *The Importance of Geometrical in the Scaffolds for Bone Reconstruction*

We can mold HAP into various geometrical shapes in the milli- and micro-meter scales during ceramic production. The desirable geometries of ceramics are crucial for inducing the cells to migrate, adhere, and grow into the normal tissues to reconstruct bone. Furthermore, we gradually understood that these 3D geometrical fabrications of HAP and related ceramic (scaffolds) were vital tools for the regeneration therapy of bone. Thus, we have developed more than twelve scaffolds of different geometry for bone formation [74–84] and classified them into eleven categories, as shown in Table 5. And we showed which geometry was practical and which was not.

This section focuses on the various geometrical scaffolds made of HAP and related ceramics and their efficacies in producing bone tissues.

Table 5 Eleven categories of geometries found in artificial ECM at micrometer level (0.1–1,000 nm). Modified from reference [74]

Categories of Geometry	Fundamental Shape		Example
Convex type	Fibers		Titanium web, Fibrous collagen membrane
	Particles		Insoluble bone Matrix, Particles with pores
Plane type	Planes		Conventional dishes
	Sheets (Membrane)		Porous sheets
	Blocks		Porous blocks of hydroxyapatite
Concave	Connected Pores		Bone is easily induced
	Straight tunnel (Honeycomb)		Rapid vasculature and bone formation
	Concavities		Bone formation on the inner surface
	Micro-pits		Cell growth at the corners
	Grooves		Directional growth of nerve cell & fibroblast
Room type	Chamber		Equipped with windows, floor & ceiling lead rapid bone formation

2.2.1 Preparation of HAP-Derived Geometrical Scaffolds

There are many fascinating methods of preparation of micro-geometrical HAP scaffolds. We classified them into two categories: molding and spacing methods. In the molding method, the paste made of HAP powders was pressed out with high pressure through the various nozzles: noodle-, macaroni-, and reverse multi-noodle-types, each of which produces rods or fibers, pipes, and honeycomb structure, respectively. We compressed the paste and let it go out from the nozzles to obtain

smaller diameters to even micron order, dried, and finally sintered to prepare geometric HAP ceramics. The spacing method, on the other hand, the HAP paste is mixed with combustible materials, such as plastic beads, fibers, or the piece of the plates with the convex dotted surface and sintered to prepare porous HAP ceramics. The temperature of sintering is usually 900–1,000°C. To our previous studies [74–83], these scaffolds induce bone effectively if they have porous structures, the pore size of which ranged 300–500 μm , which facilitate the penetration of cells.

2.2.2 Application of a Vital Growth Factor: Bone Morphogenetic Proteins (BMP)

To test the efficacy of geometric HAP scaffolds, we combined them with a bone-inducing growth factor named BMP, which Urist discovered in 1965 [84]. A remarkable characteristic of BMP was that it needed a particular scaffold to induce bone when implanted into soft tissues. Thus, to test the bone-inducing efficacy of the given scaffold, we combined it with BMP and implanted it into animal skin or muscle to see how much bone formed after 2–3 weeks.

2.2.3 Early Findings in the Geometry that Induce Bone Effectively

Historically, Reddi et al. [85] were the first to show the importance in the geometry of bone-inducing scaffold. They showed that the optimal size of granular ECM (decalcified bone powder) in BMP-induced bone formation to be around 420–850 μm in particle size. Cartilage and bone scarcely formed with the smaller particles (<74 μm). Inspired by their pioneering work, we prepared the HAP granules within which we gave the continuous and interconnected pores, and called them “porous particles of HAP,” abbreviated as PPHAP. The PPHAP induced a much higher bone induction than the granules without porosity (the smooth particles of HAP) [80].

Size and Shape of Pores

Thus, we found that the porosity of ECM is an essential determinant for tissue formation [64–66, 80], but previously there were no systematic studies.

Therefore, we systematically compared the bone-inducing efficacies by using the HAP block of the same size but five different porous pore sizes. We concluded that the optimal pore size for bone formation is 300–400 μm [81].

Concept of Optimal Spaces for Tissue Formation

We also noted generally that most of the initial bone formation started at the concave area of ECM. Furthermore, several authors have reported that bone tissue formed without the addition of BMP in the concavities and pores of ceramics *in vivo* [86].

These observations led us to the concept of “optimal spaces for tissue formation in artificial ECM.” We proposed that scaffolds had an optimal geometrical shape and size for each kind of tissue, which facilitates its cells to differentiate, proliferate, and develop tissue in a particular direction. These optimal spaces are not limited to tube- or sphere-types but include specific “spaces” between the solid ECM structures, such as fibers, particles, and flat planes. The size of the optimal spaces is assumed to be approximately 300–400 nm, which is dependent upon tissues.

The above results urged us to classify all the scaffold geometry into eleven categories, as shown in Table 5. First, the table categorized the geometries into four groups: convex-, flat-, concave-, and chamber-type. Then the convex group is divided into the fibers and particles, the flat group into the plane, sheets and blocks, and the concave group into the irregular connected pores, straight tunnel (honeycomb), concavity, micro-pits, groove, finally, the chamber type. This classification table is valuable when we design a new scaffold to regenerate certain tissues or organs because stem cells need specific geometrical circumstances to grow into the target tissue of an organ.

2.2.4 Side by Side Induction of Blood Vessel and Bone in the Tunnel Structure

In Fig. 7, we introduce an example of three-dimensional (3D) geometric artificial ECM of honeycomb-shaped ceramics with 37 tunnels made of β -TCP (Pilot Corporation, Japan). This honeycomb structure was made essentially through the unique nozzle of reverse noodle type, and extension into the micro-scale. In this bio-resorbable artificial ECM, the numbers and size of the tunnels are strictly controllable in the production process. The length of the ECM can be varied from 1 to 10 cm. Many kinds of cells and tissues can migrate into the tunnels, and develop in specific ways, dependent upon their characteristics.

There are intermediate cells between the osteoblasts and endothelial cells, which we hypothesized to be the common precursor cells for osteoblasts and endothelial cells.

We implanted the honeycomb β -TCP (3 mm in outer diameter, 4 mm in length, and 0.3 mm in tunnel size) combined with 1 mg of rhBMP-2 (a kind gift from Yamanouchi) into the subcutaneous tissue of the Wistar rat. Active vascular formation occurred along with bone formation, side by side through inside the tunnel, as shown in Fig. 8. When we looked at the enlarged view of the same sample in Fig. 9, we could see the closer relationship between erythrocytes and osteoblasts. We hypothesized the presence of common precursor cells between both cells, which we observed, but needs further verification.

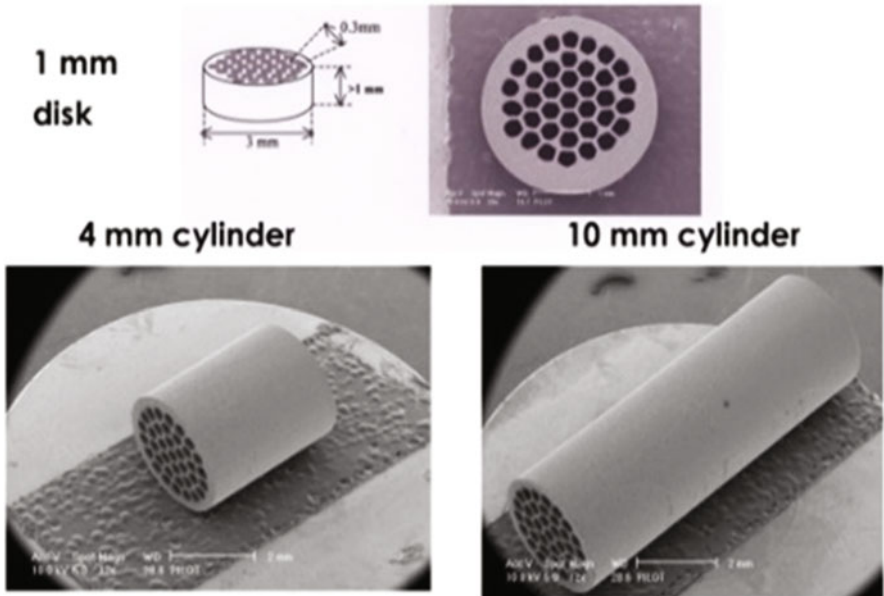


Fig. 7 An example of the geometric artificial ECM of honeycomb-shaped ceramics with 37 tunnels made of β -tricalcium phosphate (Pilot Corporation, Japan). In this bio-resorbable artificial ECM, the numbers and size of the tunnels are strictly controllable in the production process. The length of the ECM can be varied from 1 to 10 cm. Various cells and tissues can enter into the tunnels, and develop in specific ways

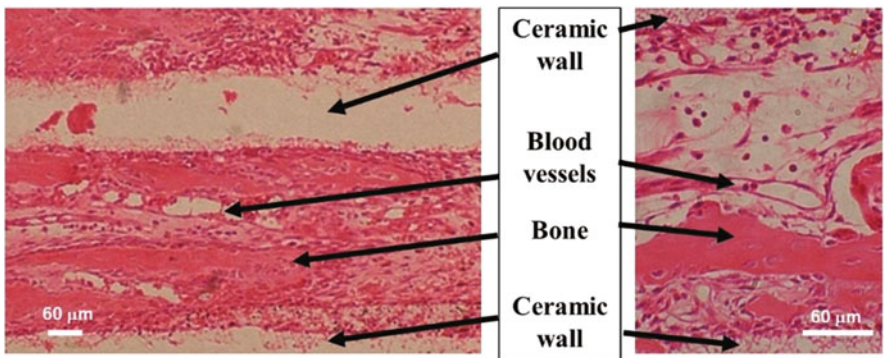


Fig. 8 Side by side induction of bone and blood vessel by the scaffold of the honeycomb structure

Furthermore, when we implanted the same honeycomb scaffolds without BMP-2, we could not observe bone formation, but only the active vascular formation, as illustrated in Fig. 10. These results indicated that the honeycomb scaffold is feasible for vascular formation, which led to bone formation when BMP supplied. This

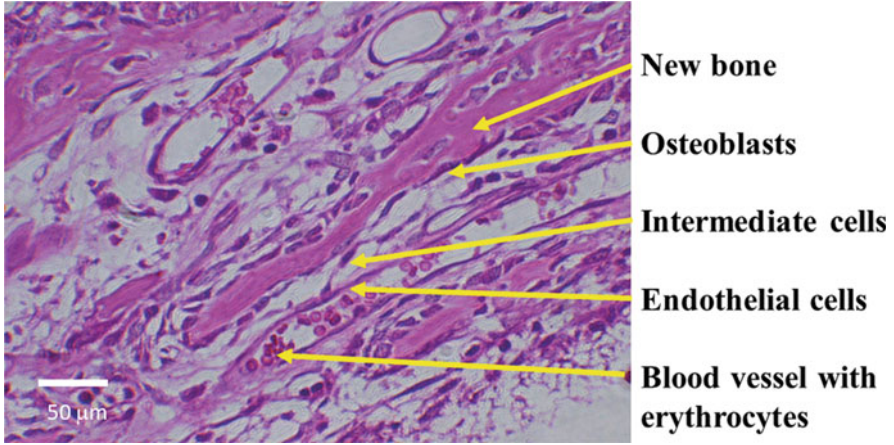


Fig. 9 Enlarged view of the relationship between the new bone and capillary

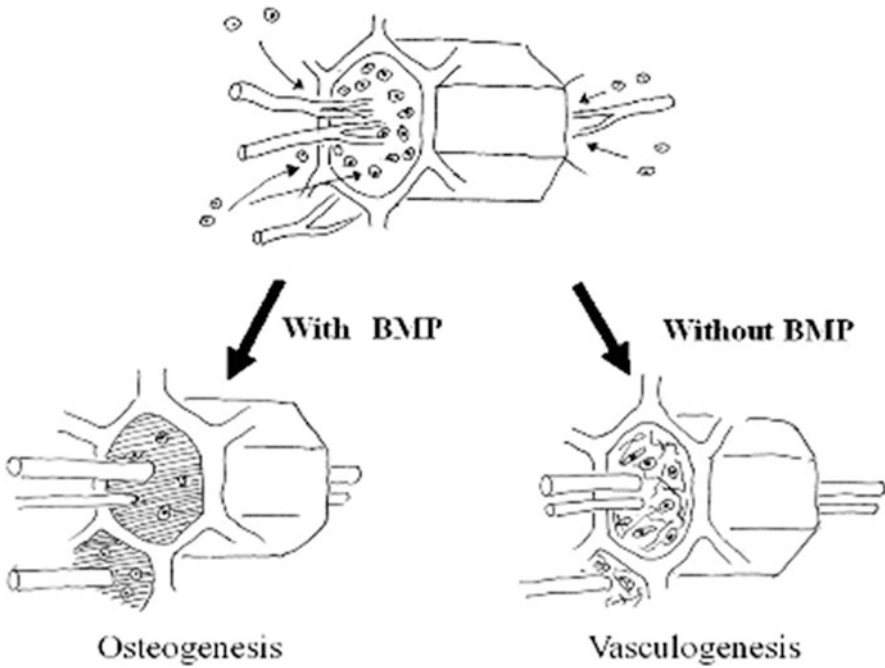
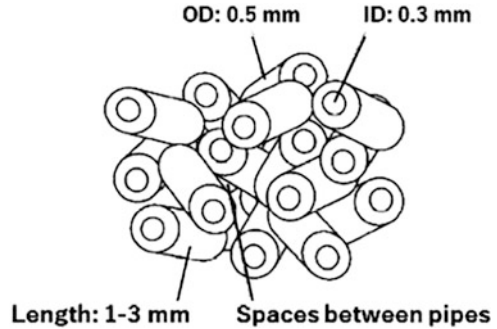


Fig. 10 Schematic explanation for the induction of osteogenesis and vasculogenesis by honeycomb scaffold

Fig. 11 Random tunnel β -TCP in that the short pipes were sintered into blocks



system of bone formation proved to be an excellent tool to clarify the relationship between blood vessels and bone formation.

Next, we extended the idea of a tunnel to the “random tunnel” β -TCP, in that the short pipes were sintered together to form the structure of random-directed tunnels. The merit of this scaffold was the increase in the 3-dimensional volume of bone formation as shown in Fig. 11.

Mechanism of Tunnel Effects

Among the 3D geometrical functions of HAP-related scaffold, tunnel-type scaffold and tunnel effect are the most eminent phenomenon. We attribute the tunnel effect to the flow of tissue fluid that facilitates cell immigration and directional growth into tissue.

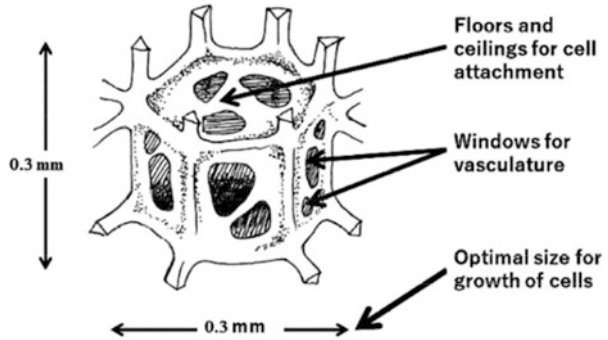
An Example of a Chamber-Type Scaffold

Figure 12 shows an example of the chamber-type scaffold that was fabricated by replicating a certain polyurethane foam, which was first calcified and sintered to a ceramic. Their geometry is proved to be ideal for bone tissue formation [74].

The above results of the geometry of scaffold indicate the common principles and recipes applicable both for the medical and environmental application of HAP-related ceramics, which we summarize as follows.

1. We studied systematically the effective geometry of scaffold for bone formation. We have divided all the geometries of ECM into three large groups: the convex-, plane- and concave-geometries, and also into the eleven practical groups. The concave geometry is generally advantageous over convex or flat, as far as the bone formation is concerned.
2. The possible mechanisms involved are as follows: (1) concave geometry permits a higher concentration of cells, (2) it leads to effective accumulation of cytokine

Fig. 12 Chamber-type scaffold that provides the osteoblasts their houses where they can grow into bone tissue



and other active bio-molecules, (3) there is a closer chance of the cell–cell communication, and (4) faster creation of three-dimensional (3D) environments, rather than two-dimensional (2D).

3. Among the concave geometries, the tunnel structures are shown to be particularly effective for bone formation. The optimal diameter of the tunnel structures was concluded to be 300–400 μm , and the effective radius of curvature is up to about 250 μm , as shown in the previous experiment.
4. These conclusions concerning the size of concave geometry are not only applicable to the tunnel structures but also may be partially eligible to open pore structures (concavities), rectangular concavities, and grooves as shown in Table 5. Furthermore, the concept of the geometry of HAP will be also applicable for use of these ceramics for water purification, which we will discuss in the next section.

2.3 Removal of Arsenate from Environmental Water by Hydroxyapatite Chromatographic System

2.3.1 Needs for Water Purification in Asian Countries

Hydroxyapatite and active carbon (charcoal) are the two effective adsorbent materials of the natural origin for environmental purification. On the other hand, it was only recently that arsenate was confirmed to exist in the raw water in Bangladesh and her vicinity. In 1998, a British scientist team reported 4,600,000–5,700,000 people (out of 122,500,000 the population of related areas) were drinking the natural well water containing more than ten ppm of arsenate, which is the maximum expected value by the WHO. The source of the arsenate is the underground water from the Himalayas [87–90]. Since the sufficient city water system is still under construction in this country, developing a low-cost and effective water purification method is very important for the local people.

Several authors have already applied HAP for the arsenate-removal method from drinking water [91–94]. But in most of their works, HAP was combined with other factors to increase the efficiency of arsenate removal, and we could not find the report in that the pure HAP was tested on the column chromatography. We developed a method of HAP chromatography for testing the arsenate removal. We synthesized hydroxyapatite (HAP) using a scallop shell as a calcium source. And we found that the shell-derived HAP could remove the arsenate effectively from water. Also, we found that the commercial bone-derived charcoal has the arsenate binding ability.

Therefore, we compared the arsenate removing abilities between the other HAP and the active carbon preparations. We have used a chromatographic system equipped with a refractive index detector. Surprisingly, we found the highest arsenate removing abilities in the hybrid of apatite and active carbon. This product was produced by carbonizing the bovine bone under the usual thermal process. This bone-derived hybrid of apatite and active carbon (abbreviated “Bone AC”) is valuable for its high arsenate-adsorbing ability. Also, we especially noticed that from the biological viewpoint of bone structure, the origin of the carbon part of this hybrid is collagen in bone. As we already described, HAP and collagen construct bone highly geometrically. This fact may cause the geometric effect of adsorption of both substances.

In this chapter, two types of HAP of biological origin: shell-derived HAP and bone apatite carbon (Bone AC) are discussed, describing their preparation methods, adsorbing function, merits for environmental water purification, and further application prospects.

2.3.2 Preparation of Hydroxyapatite from a Scallop Shell and Bovine Bone

We obtained shells of Japanese scallop (*Mizuhopecten yessoensis*) from a local fishery company in Hokkaido, Japan, cleaned of all adhering soft tissues, crushed into small pieces (<1 cm size), heated 900°C for 2 h. After cooled down to room temperature, the white product (CaO MW = 56) was transferred into distilled water at a slow step while stirring to obtain a final concentration of 9.33% (1.66 M). The homogenous suspension of Ca(OH)₂, thus prepared, is technically called lime water (pH 11).

To the 9.33% (1.66 M) lime water suspension, an equal volume of 1 M H₃PO₄ solution was slowly added stepwise with vigorous stirring. We adjusted and maintained the pH around 7.4, and we left the mixture for maturation overnight with stirring, and again adjusting pH was 7.4.

The next step is to filtrate the suspension, which was done effectively by the chromatographic system. The suspension is poured into the chromatographic column of a large scale with a 20 cm diameter, equipped with a polyester filter at the bottom, and drained the extra water. Then a sufficient volume of distilled water was added to the top of the column and drained again. We washed out all the non-reacted

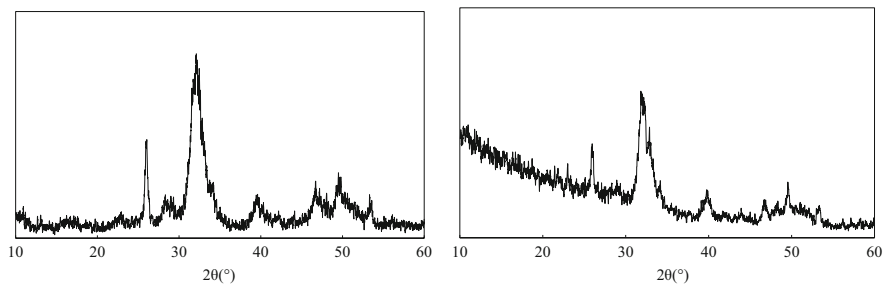


Fig. 13 X-ray diffraction patterns of the shell-derived (a) and bone-derived (b) hydroxyapatite. Both samples were analyzed by the X-ray diffraction analyzer Ultima-IV (Rigaku Corp., Japan) with a $\text{CuK}\alpha$ radiation source operating at 40 kV and a 30 mA excitation current. They showed peaks at $2\theta = 25.8^\circ$, 31.8° , and 39.8° corresponding to HAP. Analyses were done by Associate Professor Kazuhide Ozeki, Ibaraki University

soluble chemicals from the solid product, hydroxyapatite, by repeating this process. We dried the wet hydroxyapatite first in the air, then in the oven at $80\text{--}120^\circ\text{C}$. We crushed the solid mass of the dried HAP, and filtered to obtain the powder with a diameter of 1–2 mm.

Naruto Chemical Co., Tokushima, Japan, provided Bone-AC. (Commercial name: Fish-Cal). Briefly, adult bovine femora were cleaned off bone marrow and soft tissues and removed the metatarsus portions of the femora. They cleaned the hard part of bone tissue and is composed of two main components: collagen and HAP of about 25 and 65 wt.%, respectively. This raw material was processed under the usual anaerobic thermal condition and converted into Bone-AC. As mentioned in the introduction part of this article, bone collagen and HAP in the animal tissues are constructed by a unique hybrid structure with a highly ordered three-dimensional arrangement at the nanometer level [68, 95]. Since the carbon component of the Bone AC is entirely derived from the highly cross-linked type I collagen, the 3D-geometry may reflect the previous one in bone tissue, which is under investigation by SEM in this laboratory.

The products were fabricated as either fine powders of 0.05 mm or granules about 1 mm.

Figure 13a, b are the results of the X-ray diffraction analysis of Shell HAP (a) and Bone AC (b). They show the characteristic peaks at $2\theta = 25.8^\circ$, 31.8° , and 39.8° corresponding to HAP, and indicate that both samples are composed of typical hydroxyapatite of mediate crystallinity for biological origins such as bone

2.3.3 The Chromatographic Estimation of Adsorbing Ability for Arsenate

We need the rapid and straightforward method to test the various samples for adsorbing ability for arsenate and concluded that chromatography is the best one,

considering Bangladesh's present urgent environmental situation. We used a commercial glass chromatography column (Bio-Rad, Japan). We packed the various test materials into the column to obtain a $\varnothing 10 \times 50$ mm bed volume. Before packing, we removed finer particles from the test materials by repeated decantation from a suspension in distilled water. We washed the column with a large amount of distilled water and ran it at a flow rate of 80 mL/h at 15°C, using a ceramic pump (VSP-3200 W, Eyela, Tokyo, Japan). We monitored the arsenate concentration in the elution by their refraction index using a differential refraction meter (YRD-880 Shimamura Technology, Tokyo). We checked that concentrations of arsenate follow Lambert-Beer's law by the optical density and diffractive index. In addition to their refraction index, we also monitored the elution by absorbance at 254 nm with an ATTO Bio-Mini-UV monitor (Atto Co., Tokyo, Japan). We chose several HAP and active carbon preparations from different sources as the samples for testing were:

1. Shell-derived hydroxyapatite (Shell HAP),
2. Bone-derived active carbon (Bone AC),
3. Pollack bone apatite: hydroxyapatite prepared from pollack bone [Naruto Chemical (N-C) Co., Tokushima, Japan), which was designed into the particles by the method described above for scallop shell apatite.
4. Jatropha charcoal was prepared from the seeds of *Jatropha curcas* and kindly given by Jissen Kankyo Kenkyusho Co., Nagoya, Japan.

We applied a fixed amount of arsenate (As_2O_3 , 5 mg in 1 mL on the columns 10×50 mm in the bed volume), packed with different adsorbents, and ran with distilled water at a flow rate of 80 mL/h. Eluted solutions were monitored by a differential refraction meter (YRD-880 Shimamura Technology, Tokyo). Peak areas in the chromatogram were measured using Image-J software.

2.3.4 Results of as-Removal by HAPs from Shell and Bone

Figure 14 shows the chromatogram of 5 mg arsenate applied on the column 10×50 mm, which was packed with the glass beads (0.1 mm in diameters) as control of non-adsorbent material. The same arsenate amount (5 mg) was applied and ran three times successively with distilled water at the flow rate of 80 mL/h. The black arrows indicated injection points. The refractive index monitored the formers of double-peak each, and the latter was at an optical density at 254 nm. The areas of peaks were calculated using Image-J and turned out to be highly reproducible. Figure 14b shows the same chromatographic peaks of arsenate solution, except that the column was packed with the apatite beads (0.2 mm in diameters) made from scallop shells. The average peak areas of Shell HAP column (B) were 46% of glass beads column (A), which meant the remaining 54% of the charged arsenate was adsorbed in this column.

This study aimed to devise a new method to estimate the adsorption ability for arsenate of a particular material. The assay principle compares the peak areas of chromatograms produced by columns packed with glass beads (non-adsorbing

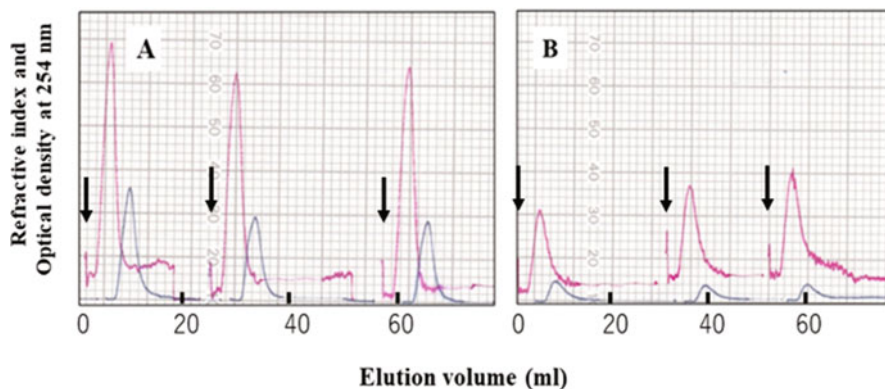


Fig. 14 Chromatographic profiles when we applied 5 mg arsenate on the column. We packed the column with the glass beads (0.1 mm in diameters) as control of non-adsorbent material (a). The same chromatographic peaks except that the column was packed with Shell-HAP (b)

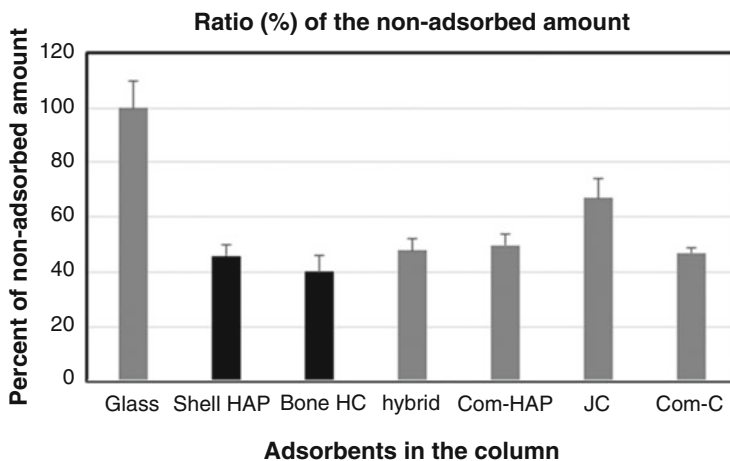


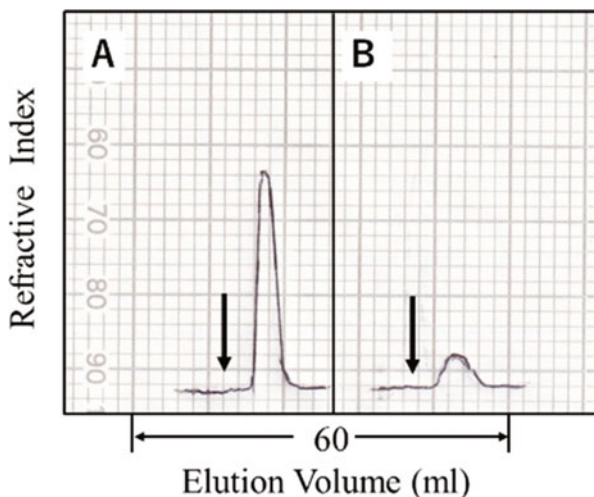
Fig. 15 Comparisons of the ratios (%) of the non-adsorbed per total applied amount of arsenate on the column packed with the different adsorbents

ability) and the testing materials. Figure 15 shows the ratios (%) of the non-adsorbed amounts per the total quantity of arsenate applied. We can estimate by comparing the peak areas of chromatograms of each sample with that of the column packed with the glass beads, which was a non-adsorbent control.

We applied the same amount of arsenate (5 mg taken as 100%), compared to the ratio of the peaks areas by Image-J, and expressed it as a percent.

Glass indicates the glass beads as a non-adsorbent control, Shell-HAP: scallop shell-derived HAP, Bone AC: Bone-derived complex of HAP and active carbon, hybrid: hybrid column packed with the commercial charcoal and commercial HAP

Fig. 16 Chromatograms of the arsenate (0.2 mg) applied on the columns packed with glass beads (a) and the bone-derived complex of HAP and active carbon (b). The peak area of B was 25% of that of a



in the upper and lower half, Com-HAP: a commercial HAP, JC: Jatropha-seed charcoal, and Com-C: commercial charcoal.

The lowest peak area (40%) indicated the highest adsorption was the bone-derived active carbon (Bone AC), which meant the highest adsorbent ability among the tested adsorbents. Other adsorbents remained within 45–50%, except for Jatropha charcoal 67%.

Figure 16 shows the chromatographic peak of 0.2 mg arsenate (2 mL of 100 ppm solution) applied on the column (10 × 50 mm), which was packed with the glass beads (0.1 mm in diameters) as control and ran at the flow rate of 120 mL/h. Figure 14b results from the same chromatography as Fig. 14a, except that the column's content was the bone-derived active carbon (Bone AC) instead of glass beads. Figure 4 showed the chromatogram with glass beads and the Bone AC on that we applied a smaller amount of arsenate (5 mg taken as 100%). Comparing the two chromatograms, we will find the peak area by the Bone AC column was 25% of glass beads. The reduction of 75% when we applied 0.2 mg was much eminent 40% when using 5 mg arsenate.

Namely, the applied amount reduced, the absorbed amount increased. We explained the reason for this situation as follows. According to the isotherm theory by Freundlich and Langmuir [96–98], the adsorbed amount of the soluble materials (adsorbate) on the solid substance (adsorbent) is dependent on the concentration of the soluble materials. The higher the concentration of the soluble materials (adsorbate), the lower the ratio of adsorbed amount/the concentration of the soluble material. The above situation occurs at least within a specific range of concentrations. Therefore, we can estimate the maximum amount of adsorbed material on a certain amount of solid materials by repeating the experiments changing the concentration of soluble materials.

We showed by chromatography that we can estimate the maximum amount of arsenate adsorbed on a certain amount of materials with adsorbing ability. The

chromatographic method we developed would be helpful for arsenate removal from water by apatite.

The mechanism of the adsorption of arsenate by HAP is an exciting issue. It is still not clear whether it is a pure adsorption phenomenon or accompanying the exchange with the atomic components of HAP. Recycling adsorbed arsenate in HAP is another promising subject.

2.4 Conclusion

1. Simple and economic adsorbing materials for arsenate (As compounds) are ardently needed in Bangladesh, where the natural well water contains arsenate originating from the Himalayas Mountains.
2. Natural sources of calcium for HAP production are available quickly, from seashell (scallop), bovine bone, pollack bone, eggshell (a hen). We propose simple methods of HAP production from these calcium resources.
3. We developed a new chromatographic method to measure the efficacy of arsenate removal from water by HAP and other materials.
4. The hybrid product of HAP and active carbon from bovine bone (bone AC) seemed to be relatively higher efficient among the HAP samples tested this time. Previously, we have no study on the bone AC for arsenate removal, and only the positive affinities of bone AC for metals: Mn, Fe, Ni, and Cu were so far reported [99]. Therefore, our first trial study of arsenate removal by bone AC is highly expected for further studies, considering the urgent water purification needs in Bangladesh.

Acknowledgements Collaborations did with Associate Professor Kazuhide Ozeki (Ibaraki University, Japan) and Dr. Iku Shouhei (Jiangsu Alphas Biological Technology Co., Ltd., Nantong, China). Their efforts are equivalent to those by Yoshinori Kuboki and Purvin Bergun, and we regarded them to possess the same authorships as us.

3 Layered Double Hydroxides (LDHs) for Removal of Drug Trace in the Environment

3.1 Introduction to Layered Double Hydroxide (LDHs)

Layered double hydroxides (LDHs) are the only known group of layered inorganic materials that have net positively charged sheets [100, 101]. Figure 17 shows a representation of the LDH layers. The layers are formed by edge sharing metal

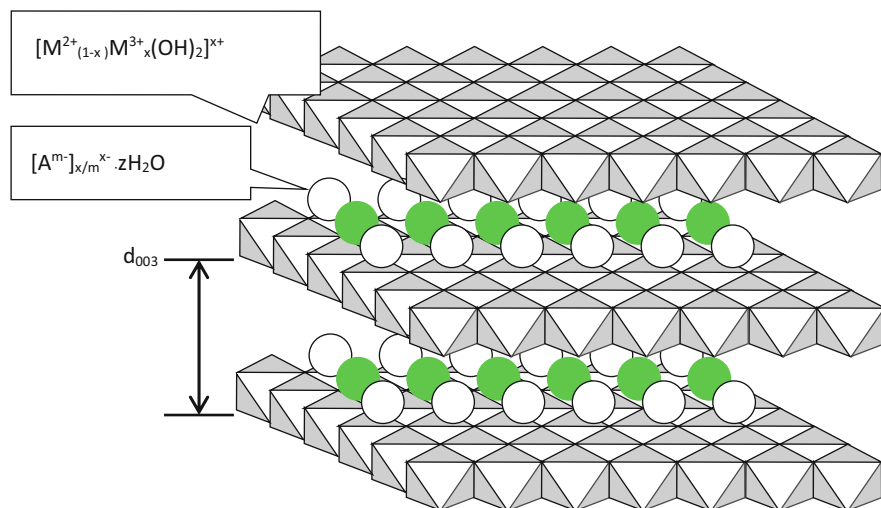


Fig. 17 Schematic structure of a layered double hydroxide. White ball: anion, green ball: water molecule

hydroxide octahedra similar to those of brucite, $Mg(OH)_2$ [102]. Substitution of some of the divalent metals by trivalent metals results in net positive charges on the layers that are neutralized by counterbalancing anions intercalated between the layers. The chemical formula of the layers can be expressed as $[M^{2+}_{(1-x)}M^{3+}_x(OH)_2][A^{m-}]_{x/m} \cdot zH_2O$ where M^{2+} and M^{3+} are di- and trivalent metals, A^{m-} is an exchangeable anion, and x normally ranges from 0.17 to 0.33 [103–105]. LDHs are also called hydrotalcite minerals, mixed metal hydroxides, or anionic clays.

A wide range of metals can form LDH layers provided certain conditions are met. First, the ionic radii of the M^{2+} and M^{3+} ions must be within 30% of each other. Second, the solubility products of the divalent metal hydroxide (S_1) and trivalent metal hydroxide (S_2) must be within 10 orders of magnitude of each other. LDHs containing divalent metals such as iron(II), magnesium, manganese(II), nickel, zinc and trivalent metals such as iron(III), aluminum, cobalt(III), and chromium(III) can be synthesized. LDHs containing monovalent and tetravalent cations such as lithium and tin(IV) have also been reported [106, 107].

Any anions or anionic complexes can function as counterbalancing species provided that they do not form complexes with the metals of the octahedral sheets during the formation of the LDH [102]. They range from inorganic anions such as CO_3^{2-} , Cl^- , SO_4^{2-} , PO_4^{3-} , polyoxometalates, etc. to organic anions such as acetate, acrylate, oxalate, benzoate, benzene sulfonate, etc. However, CO_3^{2-} is preferred and is found in almost all-natural minerals of the LDH family. Water molecules are also always found in the interlayer space. The unit cell of LDHs can contain from 1 to 6 H_2O , but usually has 4 H_2O . The prototype of the naturally occurring minerals is hydrotalcite, an Mg-Al LDH with carbonate as the charge balancing anion,

Table 6 Naturally occurring minerals with the layered double hydroxide structure

Mineral name	Empirical formula
Hydrotalcite	$Mg_6Al_2(OH)_{16}CO_3 \cdot 4H_2O$
Stichtite	$Mg_6Cr_2(OH)_{16}CO_3 \cdot 4H_2O$
Desautelsite	$Mg_6Mn_2(OH)_{16}CO_3 \cdot 4H_2O$
Pyroaurite	$Mg_6Fe_2(OH)_{16}CO_3 \cdot 4H_2O$
Reevesite	$Ni_6Fe_2(OH)_{16}CO_3 \cdot 4H_2O$
Comblainite	$Ni_6Co_2(OH)_{16}CO_3 \cdot 4H_2O$
Caresite	$(Fe^{2+}, Mg)_4Al_2(OH)_{12}CO_3 \cdot 3H_2O$
Sergeevite	$Ca_2Mg_{11}(OH)_4(CO_3)_9(HCO_3)_4 \cdot 6H_2O$
Takovite	$Ni_6Al_2(OH)_{16}(CO_3)_{0.75}(OH)_{0.25} \cdot 4H_2O$

$Mg_6Al_2(OH)_{16}CO_3 \cdot 4H_2O$. Other examples of naturally available minerals in the LDH family are listed in Table 6.

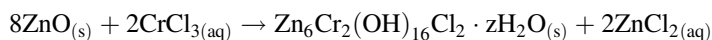
Hydrotalcite has cell parameters $a = b = 3.07 \text{ \AA}$, $\alpha = \beta = 90^\circ$, $\gamma = 120^\circ$, and $c = 23.23 \text{ \AA}$ for those with the CO_3^{2-} counter anion. Stacking of the layers can be accomplished in two ways, leading to two polytypes with a rhombohedral (3R symmetry) or a hexagonal cell (2H symmetry); hydrotalcite has 3R symmetry, while the 2H analogue is known as manasseite [102]. The density of the LDH depends on the metal cations in the layers, the interlayer anions, and the interlayer water content. For example, hydrotalcite has a density of 2.06 g/mL. The density increases to 3.05 g/mL for comblainite [102].

3.2 Syntheses of LDHs

Naturally available minerals of the LDH family are rare. Fortunately, hydrotalcite-like minerals can be synthesized very easily in the laboratory. There are numerous routes to synthetic LDHs. Some of the most significant methods will be briefly described here.

3.2.1 Salt-Oxide Method

In this method, a trivalent metal salt is added to the aqueous suspension of a divalent metal oxide. For example, Boehm and co-workers used this method in 1977 to prepare Zn-Cr-Cl LDH by adding chromium(III) chloride to the aqueous suspension of zinc oxide [103].



Zn-Al-Cl and Cu-Cr-Cl LDHs can also be synthesized using this route. Not all oxides, however, can be dispersed in the aqueous medium, limiting the range of LDHs that can be made by this method.

3.2.2 Salt-Base Method

This method, first introduced by Feicknecht in 1942, is probably the simplest [105]. It consists of the titration of the aqueous solution of a mixture of the di- and trivalent salts with a base. For example, reaction (2) shows the preparation of hydrotalcite with chloride in the interlayer space by this method.



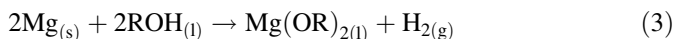
The titration itself can be performed by increasing the pH (addition of the base to the salt mixture) or decreasing the pH (addition of the salt mixture to the base). The final pH of the titration mixture must be adjusted in order to obtain well-crystallized products. Ni-Cr-Cl LDH, for example, forms well in a pH range of 3.5 to 6.8, Zn-Al-Cl LDH in a pH range of 4 to 10, Zn-Cr-Cl LDH in a pH range of 4.5 to 5, and Cu-Cr-Cl LDH at pH 5.5 [103]. In 1975, Miyata modified this method by simply adjusting the pH of the solution mixture to 10 with the base rather than by titration [105]. There was a work on LDH containing multiple metals [106].

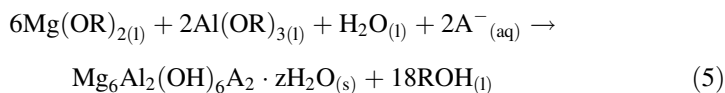
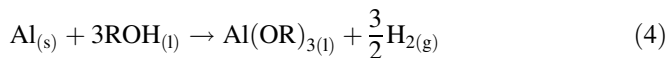
3.2.3 Stoichiometric Method

This is very similar to the salt-base method except that instead of maintaining the pH at a predetermined value, only the stoichiometric amount of the base required to form the LDH is added. For example, to produce the $\text{Mg}_6\text{Al}_2(\text{OH})_{16}\text{Cl}_2$ LDH 8 mol of NaOH is added to an aqueous solution mixture containing 3 mol of MgCl_2 and 1 mol of AlCl_3 . This is simple since no pH adjustment is required [107].

3.2.4 Metal Alcoholate Method

This method yields the very pure LDHs that are needed for some applications, such as for drug use. Heating a primary alcohol (preferably C_2 to C_{10}) and the pure metal at about 160 °C produces metal alcoholate. Hydrolysis of the metal alcoholate mixture in water containing the desired interlayer anions produces the LDHs.





This process has been patented recently [108]. However, hydrogen gas produced in these reactions needs to be handled carefully. And, some transition metals react slowly with alcohol limiting the range of LDHs that can be prepared. There are methods generally employed for the synthesis of transition metal alkoxides [109] that could probably be used to prepare LDHs.

3.2.5 Heat Treatment of Metal Oxides Suspensions

Heating a mixture of metal oxides with a small amount of water at elevated temperatures, about 450–500 °C, in an oxygen free environment will produce a slurry of LDH precursors. Hydrolysis of the slurry at room temperature in an aqueous medium containing the desired anion gives LDHs with good crystallinity. MgO and Al₂O₃ have been successfully converted into LDH using this method [110]. The hydrolysis can be done at room temperature. As of the salt-oxide method, the difficulty is to develop a good aqueous suspension of the precursors. This limits this method to the synthesis of LDHs containing main group metals.

3.3 Anion Exchange Properties of LDHs

The counterbalancing anions in the LDH interlayer are exchangeable. LDHs are one of the main classes of inorganic anion exchangers. Thermodynamically, ion exchange in the LDH depends mainly on the electrostatic interactions between positively charged hydroxylated sheets and the exchanging anions, and on the free energy involved in the changes of the hydration state of these ions. The equilibrium is constant for adsorption increases with the decrease of the ionic radius of the unhydrated (bare) anion. Ion exchange is therefore favored for incoming anions with a high charge density. In 1983, Miyata suggested a comparative list of ion selectivity for monovalent anions as $\text{OH}^- > \text{F}^- > \text{Cl}^- > \text{Br}^- > \text{NO}_3^- > \text{I}^-$, and for divalent anions $\text{CO}_3^{2-} > \text{C}_{10}\text{H}_4\text{N}_2\text{O}_8\text{S}^{2-} > \text{SO}_4^{2-}$. For oxoanions the order is HPO_4^{2-} ; $\text{HAsO}_4^{2-} > \text{CrO}_4^{2-} > \text{SO}_4^{2-} > \text{MoO}_4^{2-}$ [111]. According to these guidelines, nitrate-LDHs and iodide-LDHs are the best anion exchangers. Also, the selectivity for divalent anions is higher than for monovalent anions.

Although LDHs have complementary structures to the smectite clays, they are not easily pillared [3]. They have relatively high layer charge density ($\sim 0.04 \text{ e}^+/\text{X}^2$ for LDHs versus $0.01 \text{ e}^-/\text{X}^2$ for smectites) [3]. Thus, the galleries of the LDHs tend to

become crowded with the pillaring anions themselves. Nonetheless, polyoxometalate anions that have high charge density have been found effective in pillaring LDHs. The pillaring ions, however, must have a high negative charge density to balance the high positive charge density of the octahedral sheets, and be stable to hydrolysis reactions at above neutral pH. The first polyoxometalate ion that was successfully intercalated into the LDH gallery was $V_{10}O_{28}^{6-}$ by using Zn_2Al , Zn_2Cr , and Ni_3Al LDHs [111]. Keggin ions, $[X^{n+}M_{12}O_{40}]^{(8-n)-}$, have also shown a possibility to occupy the interstitial space. Anions formed at a lower pH require LDHs that are stable at a lower pH. Recently, Mg-Al LDH pillared with the decamolybdodicobaltate(III)anion, $[H_4Co_2Mo_{10}O_{38}]^{6-}$, has been found to remain intact at a pH as low as 4.7 [112].

3.4 Common Applications

LDHs have been used in various fields. Very pure synthetic Mg-Al- CO_3 layered double hydroxides have found applications as a pharmaceutical antacid (Talcid® by Bayer, Germany, and Altacite® by Peckforton Pharmaceuticals Ltd., England). These LDH-based antacids are especially good for patients that also suffer from hypertension and diabetes because of their low sodium and calcium contents. Another potential use of LDHs in the pharmaceutical industry is in drug delivery systems, especially for anionic drugs such as Ibuprofen. Mg-Al-Ibuprofen can be prepared by the ion exchange of Mg-Al-Cl LDH. The drug can then be slowly released into the digestive tract as the LDH framework dissolves in the gastric fluid to prolong the pharmacologic effect of the drug [113].

Another promising application of the LDHs is as gene reservoirs. Phosphate groups in DNA double helices that have negative charges can form weak ionic bonds with the positively charged sheets of LDHs [114]. The DNA stored in the LDH interlayer space can be released back into the aqueous solution simply by lowering the pH of the system.

There are numerous reports on the use of LDHs in organic syntheses as catalysts and catalyst supports. The recent work by Choudory et al. showed that the tetrachloropaladate anion could be intercalated into the LDH interlayer to produce catalysts for Heck-, Suzuki-, and Stille-coupling reactions with excellent yields [115]. Mg-Al hydrotalcite itself has been found to catalyze the reaction between aldehydes and nitroalkanes to afford nitroalkanols. Mg-Al-O-t-Bu LDH is an efficient catalyst for the 1,4-Michael addition [116]. Ruthenium-grafted LDHs are good catalysts for direct alpha-alkylation of nitriles with primary alcohols [117]. LDHs with OsO_4^{2-} counterbalancing anion have been prepared as catalysts for asymmetric dihydroxylation of olefins to vicinal diols [118] and LDHs with MnO_4^- for alcohol oxidation. In environmental remediation, Cu-Mg-Al LDH has proven to be a new catalyst for the simultaneous removal of SO_x and NO_x , gases that cause acid rain [119].

One large-scale application of LDHs is as polymer additives. They are used in polyolefin syntheses to neutralize residual acidic substances from Ziegler-Natta or other polymerization catalysts. The addition of the LDHs to the polymers prevents degradation and improves their heat and weathering resistance. They have been used in the stabilization of halogen containing polymers, particularly polyvinylchloride (PVC) [120], where they function as scavengers for the HCl released from the PVC. This is an excellent development since most acid scavengers are generally made of compounds containing lead, tin, or barium. LDHs that have carbonate and acrylate in the interlayer space are particularly good fire retardants. Some new materials based on polymer-LDH nanocomposites have begun to be studied. Polyacrylate-LDH nanocomposite might be useful in the design of fireproof material. Conducting polymers such as doped polyaniline, polythiophene, and polyacetylene are prospective candidates for electronic applications and can be inserted into the LDH interlayer to obtain a desirable range of electrical conductivity [121].

3.4.1 LDH for Removal of Drug Traces in the Environment

Research on the application of layered double hydroxide (LDH) as an anion exchanger in the pharmaceutical field is still being developed. The pharmaceutical drugs and their metabolites are a subclass of detectable organic contaminants in wastewater, and aquatic environments, the concentration of which keeps increasing. A diverse group of pharmaceuticals, potential endocrine disrupting compounds (EDCs), and other unregulated organic contaminants were screened. The 11 most frequently detected compounds in the US drinking water were atenolol, atrazine, carbamazepine, estrone, gemfibrozil, meprobamate, naproxen, phenytoin, sulfamethoxazole, TCEP, and trimethoprim [122]. Antibiotics are the focus of many studies because of the high frequency of detection in the environment and the increased incidence of bacterial resistance. Nowadays, there is increasing use of antibiotics as means of treating infectious diseases, especially those caused by microorganisms. Surveys conducted within the country and abroad found that β -lactam antibiotics are the most widely prescribed antibiotics. Amoxicillin is semisynthetic penicillin that has antibiotic properties of the β -lactam ring. The increased presence of β -lactam antibiotics such as amoxicillin in aquatic environments will lead to reduced water quality, be a threat to ecosystems, and affect the quality of drinking water source [123].

Several studies on the application of LDH as anion exchanger in the pharmaceutical field have been widely reported, e.g., the application of Ni-Al-NO₃ LDH in the determination of salicylic acid in blood serum, willow leaves, and aspirin tablets [124]. The extracts of salicylic acid were measured using spectrofluorometry with obtained percent recovery of 96–101%. Other works have been carried out in the determination of mesalamine content in human serum through the process of preconcentration by SPE with Ni-Al LDH as an anion exchanger and obtained percent recovery of up to 99% [125]. Ni-Al-NO₃ LDH as an anion exchanger was reported to have successfully analyzed the level of mefenamic acid in human serum

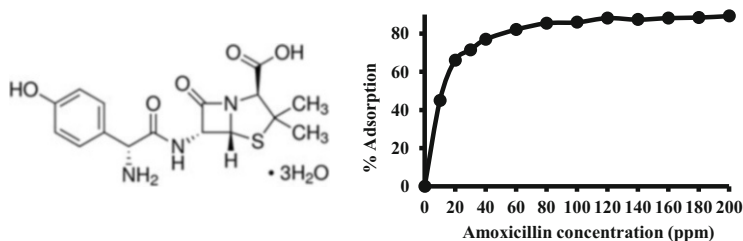


Fig. 18 Chemical structure of amoxicillin and adsorption profile of amoxicillin by Mg-Al LDH

and pharmaceutical wastewater samples and gave results between 94.7 and 104%. Mg-Al-diclofenac LDH has been successfully prepared by the ion-exchange method with initial CO_3^- anion present in the LDH [126]. The adsorption capacity of the calcined hydrotalcite was about 1.9 mmol g^{-1} .

One good example of LDH application is in the removal of antibiotic drug in the environment. Amoxicillin (Am) drug has been successfully intercalated into the interlayer of Mg-Al hydrotalcite through anion exchange [127]. Amoxicillin in slight alkaline media has a negative charge. Mg-Al- NO_3 LDH was synthesized, exchanged with oxalate ion, and applied as an adsorbent for amoxicillin. Figure 18 shows the structure of the compound and the adsorption reaction, whereas Fig. 19 displays the XRD and FTIR data. The process of amoxicillin adsorption is carried out through an ion-exchange method. The XRD of the Mg-Al- NO_3 , Mg-Al-Ox, and Mg-Al-Am is displayed. The Mg-Al- NO_3 LDH gives 2 θ peaks at 11.34° , 23.07° , and 34.55° . They correspond to the $d_{(003)}$, $d_{(006)}$, and $d_{(009)}$ spacings, respectively. It confirms the data reported in the previous works. The XRD pattern could be fitted to the hexagonal phase of a typical Mg-Al LDH (JCPDS file 22-0700). After ion exchange with oxalate, the diffraction peak at 2θ 5.33° is detected. It is also consistent with the data in the literature for LDH with oxalate ion. The Mg-Al-Am LDH gives diffraction peaks at 2θ 8.9° and 18.1° , corresponding to the $d_{(006)}$ and $d_{(009)}$ spacing and gives large basal spacing to indicate the insertion of the drug.

The FTIR spectra of Mg-Al- NO_3 , Mg-Al-Ox before and after the exchange are shown in Fig. 19. The band at $3,400\text{--}3,500 \text{ cm}^{-1}$ could be assigned as an O-H stretching vibration of the LDH octahedral layer and water molecules in the interlayer. For Mg-Al- NO_3 LDH, there is a weak band at $1,620 \text{ cm}^{-1}$, which could be associated with O-H bending vibrations. A sharp peak that appears at $1,381 \text{ cm}^{-1}$ may be attributed to NO_3^- asymmetric stretching vibration. According to the previous study, the LDH-FTIR spectra give a band at $3,463 \text{ cm}^{-1}$, which could be ascribed as an O-H vibration mode of free water molecules, M-OH lattices, and interlayer water molecules. The peak at $1,635 \text{ cm}^{-1}$ is the corresponding bending vibration of O-H. The band at $1,381 \text{ cm}^{-1}$ could be attributed to the asymmetric stretching vibration of nitrate ions. The peaks detected at 617 , 447 , and 409 cm^{-1} could be due to the stretching vibration of M-O. After ion exchange, the NO_3^- asymmetric vibration is no longer seen. In the Mg-Al-Ox LDH spectrum, the peaks that appear at $1,635 \text{ cm}^{-1}$ could be attributed to the C=O vibration mode. The appearance at $1,389 \text{ cm}^{-1}$ is due to the C-O asymmetric stretching of carboxylate

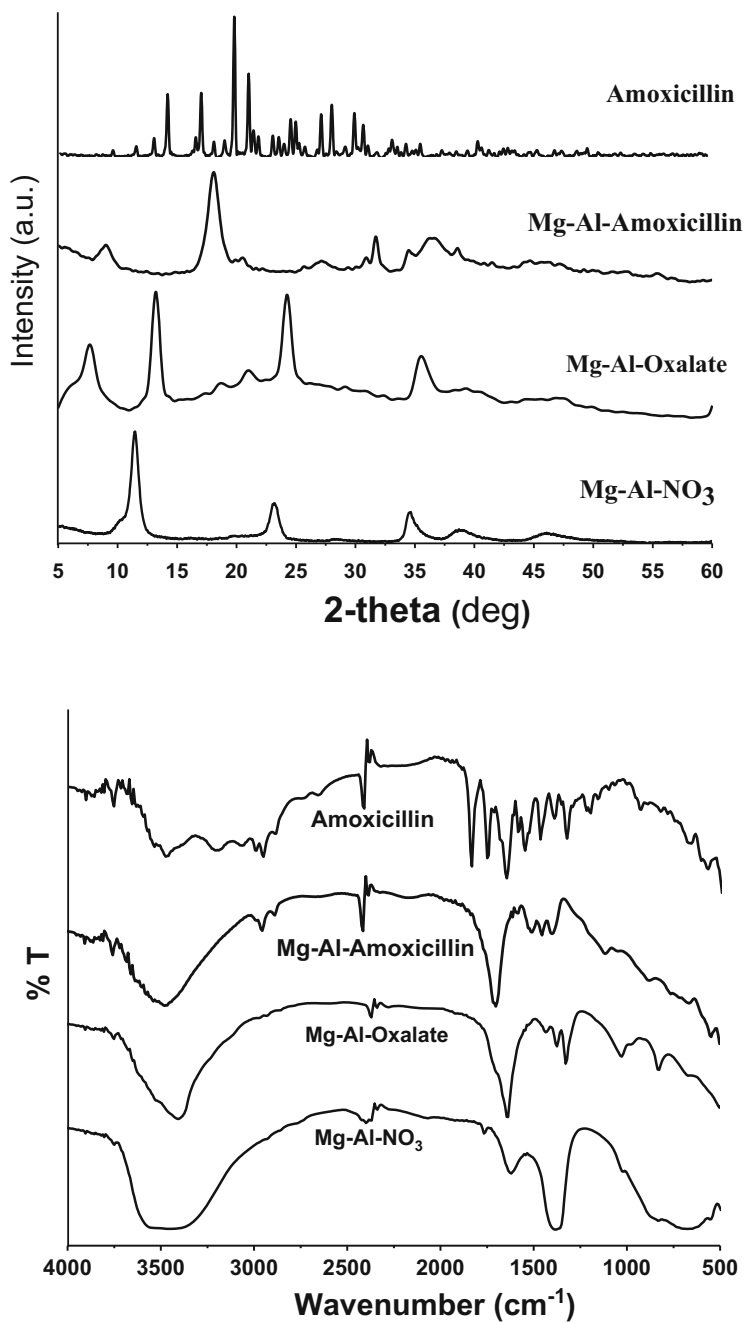


Fig. 19 XRD pattern and FTIR of Mg-Al LDH before and after adsorption of amoxicillin

ions. Multiple peaks in the fingerprint region of 400–800 cm^{-1} are believed to be due to the bending vibrations of the metal oxide of Mg-O, Al-O, Mg-O-Al, and O-Mg-O or O-Al-O.

After ion exchange, the peaks at 2,924, 1,774, 1,690 cm^{-1} might be assigned as the stretching vibration modes of the C_{sp^3} -H, C=O, and C=C bonds of the drug, respectively. The peaks observed at 1,582, 1,481, and 1,090–1,020 cm^{-1} could be assigned as bending vibration modes of the N-H, C-H, and C-N bonds. The bending vibration modes of the C-H and C-S are viewed at 1,000–675 and 563 cm^{-1} , respectively. The peak at 3,071 cm^{-1} is believed to be the stretching vibration mode of the benzene C_{sp^2} -H bond. Also, the peaks at 1,597 and 1,543 cm^{-1} could be attributed to the vibration mode of the benzene ring. It means that the amoxicillin has replaced the oxalate ion. All these prove that trace amoxicillin in the environment could be immobilized by the use of layered double hydroxides. Other negatively charged drug molecules may have similar interactions.

4 Conclusion

It has been demonstrated in this chapter that coal bottom/fly ash, hydroxyapatite, and hydrotalcite are potential inorganic materials that can be modified and applied in many applications such as environmental remediation and health areas. Coal ash can be found naturally and is normally classified as hazardous waste of coal burn, because of its high content of silica and alumina, it can be activated and modified to become selective adsorbents of heavy metals and dyes, so it can support zero-waste policy as well as innovation motto “form pollution to solution.” Hydroxyapatite and hydrotalcite are all environmentally benign materials. Both of them are also easy to prepare. Further modification and activation may be required to solve the target environmental and health issues. These can be basically achieved by considering the phenomena underlying the process such as the interaction between adsorbent and the target molecules and the properties of both the active site of the adsorbents and adsorbates as described in some examples of applications given in this chapter. In the future, these three types of materials may be modified further to address the developed environmental issues as well as to explore their possible applications in supporting many areas such as health, medicinal, and agricultural issues as multifunctional materials.

References

1. Jumaeri J (2015) Synthesis of zeolite A from coal fly ash and its modification using HDTMAB as a multifunctional adsorbent. PhD Disertasi, Chemistry Department Gadjah Mada University, Yogyakarta, Indonesia
2. Hessley RK, Reasoner JW, Riley JT (1986) Coal Science. Wiley, New York, pp 81–87

3. Oplis N (2014) Coal use and growth development potential of the economy. <http://Funwithgovernment.blogspot.com>
4. Kikuchi R (1999) Application of coal ash to environmental improvement transformation into zeolite, potassium fertilizer and FGD absorbent. *J Res Conserv Recycl* 27:333–346. <http://hdl.handle.net/1975/211>
5. Kula I, Olgun A, Erdogan Y, Sevinc V (2000) Effect of colemanite waste, coal bottom ash and fly ash on the properties of cement. *Cem Concr Res* 32:491–494. [https://doi.org/10.1016/s0008-8846\(00\)00486-5](https://doi.org/10.1016/s0008-8846(00)00486-5)
6. Mukhtar S, Kenimel AL, Sadaka SS, Mathis JG (2002) Evaluation of bottom ash and composite manur blends as a soil amandement material. *J Bioresour Technol* 89:217–228. [https://doi.org/10.1016/s0960-8524\(03\)00085-3](https://doi.org/10.1016/s0960-8524(03)00085-3)
7. Kuncoro MP, Fahmi MZ (2013) Removal of Hg and Pb in aqueous solution using coal fly ash adsorbent. *J Procedia Earth Planet Sci* 6:377–382. <https://doi.org/10.1016/j.proeps.2013.01.049>
8. Sunarti (2008) Preparation of modified adsorbent from coal bottom ash and its application for adsorption of heavy metal lead (Pb). M.Sc. thesis, Chemistry Department, Gadjah Mada University, Yogyakarta, Indonesia
9. Londar E, Fansuri H, Widiastuti N (2010) Effect of carbon on the formation of zeolite from bottom ash by direct hydrothermal method. Master thesis, Surabaya Institute of Technology, Surabaya, Indonesia
10. Wicaksono D (2014) Competitive adsorption of methylene blue and methyl orange using coal base ash. B.Sc. final project, Chemistry Department, Gadjah Mada University, Yogyakarta, Indonesia
11. Anderson AM, Rubin JA (1981) Adsorption of inorganics at solid-liquid interfaces. An Arbor Science Publishers
12. Tanjungsari R (2008) Pb(II) metal ion adsorption study by coal bottom ash. B.Sc. final project, Chemistry Department, Gadjah Mada University, Yogyakarta, Indonesia
13. Jati RA (2012) Methylene blue and methyl orange adsorption using coal bottomash in a binary system. B.Sc. final project, Chemistry Department, Gadjah Mada University, Yogyakarta, Indonesia
14. Septiana A (2013) Adsorption study of Pb(II), Cu(II) and Cr(II) metal ions using coal bottom ash. B.Sc. final project, Chemistry Department, Gadjah Mada University, Yogyakarta, Indonesia
15. Murniati M (2009) Preparation of zeolite from coal bottom ash and its application as Cu (II) adsorbent. M.Sc. thesis, Chemistry Department, Gadjah Mada University, Yogyakarta, Indonesia
16. Sutarno S, Arryanto Y, Yulianto I (2000) Utilization of fly ash waste as a basic material for faujisite synthesis with hydrothermal interaction smelting method. In: Proceedings of the 8th national chemistry seminar, Gadjah Mada University, Yogyakarta, Indonesia. pp. 265–270
17. Ratnasari M, Widiastuti N (2011) Adsorption of Cu(II) metal ions on zeolite synthesized from coal base ash of PT IPMOMI paiton by column method. In: Proceedings of the Unesa chemistry national seminar
18. Jundu R (2012) Thermodynamics of simultaneous adsorption of Mg(II) and Ca(II) influenced by heavy metals on dithizone modified silica gel. www.wordpress.com. Accessed 10 Feb 2014
19. Padi P (2009) The effect of HCl treatment on the character of klaten natural zeolite. M.Sc. thesis, Chemistry Department, Gadjah Mada University, Yogyakarta, Indonesia
20. Mufrodi Z, Sutrisno B, Hidayat A (2011) Modification of fly ash waste as a new adsorbent material. In: Proceedings of the chemical engineering national seminar
21. Wahyuni S, Widiastuti N (2009) Zn(II) metal ion adsorption on zeolite A synthesized from coal base ash of PT IPMOMI paiton with batch method. In: Proceeding of 2008 final project, Surabaya Institute of Technology, Surabaya, Indonesia

22. Yao ZT, Ji XS, Sarker PK, Tang JH, Ge LG, Xia MS, Xi YQ (2015) A comprehensive review on the applications of coal fly ash. *Earth-Sci Rev* 141:105–121. <https://doi.org/10.1016/j.earscirev.2014.11.016>
23. Matzenbacher CA, Garcia ALH, Dos Santos MS, Nicolau CC, Premoli S, Correa DS, De Souza CT, Niekraszewicz L, Dias JF, Delgado TV (2017) DNA damage induced by coal dust, fly and bottom ash from coal combustion evaluated using the micronucleus test and comet assay in vitro. *J Hazard Mater* 324:781–788. <https://doi.org/10.1016/j.jhazmat.2016.11.062>
24. Mushtaq F, Zahid M, Bhatti IA, Nasir S, Hussain T (2019) Possible applications of coal fly ash in wastewater treatment. *J Environ Manag* 204:27–46. <https://doi.org/10.1016/j.jenvman.2019.03.054>
25. Dindi A, Quang DV, Vega LF, Nashef E, Abu-Zahra MRM (2019) Applications of fly ash for CO₂ capture, utilization, and storage. *J CO₂ Util*:82–102. <https://doi.org/10.1016/j.jcou.2018.11.011>
26. Valer MMM, Lu Z, Zhang Y, Tang Z (2008) Sorbents for CO₂ capture from high carbon fly ashes. *Waste Manag* 28:2320–2328. <https://doi.org/10.1016/j.wasman.2007.10.012>
27. Kanarac M, Dolic M, Veljonic D, Ognjanovic VR, Velickovic Z, Pavicevic V, Marinkovic A (2018) The removal of Zn²⁺, Pb²⁺, and As(V) ions by lime activated fly ash and valorization of the exhausted adsorbent. *J Waste Manag* 78:366–378. <https://doi.org/10.1016/j.wasman.2018.05.052>
28. Xiyili H, Cetintas S, Bingol D (2017) Removal of some heavy metals onto mechanically activated fly ash: modeling approach for optimization, isotherms, kinetics and thermodynamics. *Process Saf Environ PRO* 109:288–300. <https://doi.org/10.1016/j.psep.2017.04.012>
29. Serrano D, Kwapinska M, Sánchez-Delgado S, Leahy JJ (2018) Fly ash characterization from *Cynara Cardunculus* L. Gasification. *Energy Fuels* 32(5):5901–5909. <https://doi.org/10.1021/acs.energyfuels.7b04050>
30. Sari DK, Setyaningsih EP, Fansuri H, Susanto TE (2018) Study of the chemical and physical characteristics of fly ash which determines the mechanical strength of fly ash based geopolymer adhesives. *Akta Kimindo* 3(2):222–235
31. Wang N, Zhao Q, Zhang A (2017) Catalytic oxidation of organic pollutants in wastewater via a fenton-like process under the catalysis of HNO₃-modified coal fly ash. *RSC Adv* 7:27619–27628. <https://doi.org/10.1039/C7RA09925H>
32. Blissett R, Rowson N (2012) A review of the multi-component utilisation of coal fly ash. *Fuel* 97:1–23. <https://doi.org/10.1016/j.fuel.2012.03.024>
33. Giribabu P, Swaminathan G (2016) Synergetic degradation of reactive dye acid red-1 by cobalt-doped lignite fly ash. *Desalin Water Treat* 57:16955–16962. <https://doi.org/10.1080/19443994.2015.1082509>
34. Ji L, Yu H, Wang X, Grigore M, French D, Gözükarar YM, Yu J, Zeng M (2017) CO₂ sequestration by direct mineralisation using fly ash from Chinese Shenfu coal. *Fuel Process Technol* 156:429–437. <https://doi.org/10.3390/cryst11111314>
35. Wu H, Zhu Y, Bian S, Ko JH, Li SM, Xu Q (2018) H₂S adsorption by municipal solid waste incineration (MSWI) fly ash with heavy metals immobilization. *Chemosphere* 195:40–47. <https://doi.org/10.1016/j.chemosphere.2017.12.068>
36. Kumar THV, Sivasankar V, Fayoud N, Oualid HA, Sundramoorthy AK (2018) Synthesis and characterization of coral-like hierarchical Mgo incorporated fly ash composite for the effective adsorption of azo dye from aqueous solution. *Appl Surf Sci* 449:719–728. <https://doi.org/10.1016/j.apsusc.2018.01.060>
37. Patra G, Barnwal R, Bahera SK, Meikap BC (2018) Removal of dyes from aqueous solution by sorption with fly ash using a hydrocyclone. *J Environ Chem Eng* 6:5204–5211. <https://doi.org/10.1016/j.jece.2018.08.011>
38. Pura S, Atun G (2009) Adsorptive removal of acid blue 113 and tartrazine by fly ash from single and binary dye solutions. *Sep Sci Technol* 44:75–101. <https://doi.org/10.1080/01496390802437057>

39. Alouani ME, Achhouri ME, Taibi M (2017) Potential use of moroccan fly ash as low cost adsorbent for the removal of two anionic dyes (indigo carmine and acid orange). *J Mar Sci Eng* 8(9):3397–3409. <https://www.jmaterenvironsci.com>
40. Jimping LI, Jinhua G, Liang W, Juan Y (2016) Preparation of fly ash based adsorbents for removal active red X-3B from dyeing wastewater. *MATEC Web Conf* 67:07004. <https://doi.org/10.1051/mateconf/20166707004>
41. Atun G, Ayar N, Kurtoglu AE, Ortabay S (2019) A comparison of sorptive removal of anthraquinone and azo dyes using fly ash from single and binary solutions. *J Hazard Mater* 371:94–107. <https://doi.org/10.1016/j.jhazmat.2019.03.006>
42. Liu J, Mwamulima T, Wang Y, Fang Y, Song S, Peng C (2017) Removal of Pb(II) and Cr (VI) from aqueous solutions using the fly ash-based adsorbent material-supported zero-valent iron. *J Mol Liq* 243:205–211. <https://doi.org/10.1016/j.molliq.2017.08.004>
43. Soni R, Shukla DP (2019) Synthesis of fly ash based zeolite-reduced graphene oxide composite and its evaluation as an adsorbent for arsenic removal. *Chemosphere* 219:504–509. <https://doi.org/10.1016/j.chemosphere.2018.11.203>
44. Feng W, Wan Z, Daniels J, Li Z, Xiao G, Yu J, Xu D, Guo H, Zhang D, May EF, Li G (2018) Synthesis of high quality zeolites from coal fly ash: mobility of hazardous elements and environmental applications. *J Clean Prod* 202:390–400. <https://doi.org/10.1016/j.jclepro.2018.08.140>
45. Zhuannian L, Anning Z, Guirong W, Xiaoguang Z (2009) Adsorption behavior of methyl orange onto ultrafine coal powder. *Chin J Chem Eng* 17(6):942–948. <http://cjche.cip.com.cn>
46. Jarusiripot C (2014) Removal of reactive dye by adsorption over chemical pretreatment coal based bottom ash. *Procedia Chem* 9:121–130. <https://doi.org/10.1016/j.proche.2014.05.015>
47. Valaskova M, Martynkova GS, Matejka V, Kratosova G (2007) Chemically activated kaolin-ites after deintercalation of formamide. *Ceramics-Silikaty* 51(1):24–29
48. Terrazas CGD, Ibarra RJ, Ortiz-Méndez U, Torres-Martínez LM (2005) Iron leaching of a Mexican clay of industrial interest by oxalic acid. *Adv Technol Mat Mat Process* 7(2): 161–166. <https://doi.org/10.2240/azojomo0168>
49. Wang Y, Ren D, Zhao F (1999) Comparative leaching experiments for trace elements in raw coal, laboratory ash, fly ash and bottom ash. *Int J Coal Geol* 40:103–108. <http://www.paper.edu.cn>
50. Suseno S (2006) Physical immobilization of dithizone in natural zeolite and study of its adsorption ability towards Pb(II) and Cd(II) metals. M.Sc. thesis, Chemistry Department, Gadjah Mada University, Yogyakarta, Indonesia
51. Kunarti ES (1994) Formation and chromatographic separation characteristics of diethylthiocarbamate and dithizonate complex compounds. M.Sc. thesis, Chemistry Department, Gadjah Mada University, Yogyakarta, Indonesia
52. Wogo HE, Segu JO, Ola P (2011) Synthesis of dithizone immobilized silica gel through sol gel process. *J Sci Appl Chem* 5:84–95. <https://ppjp.ulm.ac.id/journal/index.php/jstk>
53. Cestari AR, Vieira EF, Lopes EC, Silva RA (2004) Kinetics and equilibrium parameters of Hg (II) adsorption on silica-dithizone. *J Colloid Interf Sci* 272:271–276. <https://doi.org/10.1016/j.jcis.2003.09.019>
54. Salih B, Denizli B, Kavakli C, Say R, Piskin E (1998) Adsorption of heavy metal ions onto dithizone-anchored poli(EGDMA-HEMA) microbeads. *Talanta* 46:1205–1213. [https://doi.org/10.1016/S0039-9140\(97\)00362-7](https://doi.org/10.1016/S0039-9140(97)00362-7)
55. Absalan G, Goudi AA (2004) Optimizing the immobilized dithizone on surfactant-coated alumina as a new sorbent for determination of silver. *Sep Purific Technol* 38:209–214. <https://doi.org/10.1016/j.seppur.2003.11.008>
56. Savafi A, Bagheri M (2004) Design and characteristics of a mercury(II) optode based on immobilization of dithizone on a triacetylcellulose membrane. *Sensor Actuat B* 99:608–612. <https://doi.org/10.1016/j.snb.2004.01.022>

57. Savafi A, Bagheri M (2005) Design of a copper(II) optode based on immobilization of dithizone on a triacetylcellulose membrane. *Sensor Actuat B* 107:53–58. <https://doi.org/10.1016/j.snb.2004.10.062>
58. Mudasir M, Raharjo G, Tahir I, Wahyuni ET (2008) Imobilization of dithizone onto chitin isolated from prawn seawater shells (*P.marguensis*) and preliminary study for the adsorption of Cd(II) ion. *J Phys Sci* 19:63–78. <https://jps.usm.my/wp-content/uploads/2014/11/Article-19-1-6.pdf>
59. Yu HM, Song H, Chen ML (2011) Dithizone immobilized silica gel on-line preconcentration of trace copper with detection by flame atomic absorption spectrometry. *Talanta* 85:625–630. <https://doi.org/10.1016/j.talanta.2011.04.039>
60. Rohyami Y (2011) Study of Cu(II) preconcentration with solid phase extraction method using dithizone immobilized chitin as adsorbent. M.Sc. thesis, Chemistry Department, Gadjah Mada University, Yogyakarta, Indonesia
61. Mudasir M, Karelius K, Aprilita NH, Wahyuni ET (2016) Adsorption of mercury(II) on dithizon-immobilized natural zeolite. *J Environ Chem Eng* 4:1839–1849. <https://doi.org/10.1016/j.jece.2016.03.016>
62. Mudasir M, Baskara RA, Suratman A, Yunita KS, Perdana R, Puspitasari W (2020) Simultaneous adsorption of Zn(II) and Hg(II) ions on selective adsorbent of dithizone-immobilized bentonite in the presence of Mg(II) ion. *J Environ Chem Eng* 8:104002. <https://doi.org/10.1016/j.jece.2020.104002>
63. Huda BN, Wahyuni ET, Mudasir M (2021) Eco-friendly immobilization of dithizone on coal bottom ash for the adsorption of lead(II) ion from water. *Results Eng* 10:100221. <https://doi.org/10.1016/j.rineng.2021.100221>
64. Aminy DE, Rusdiarso B, Mudasir M (2021) Adsorption of Cd(II) ion from the solution using selective adsorbent of dithizone-modified commercial bentonite. *Int J Environ Sci Technol*. <https://doi.org/10.1007/s13762-021-03570-1>
65. Kato Y et al (2003) Biomineralization (BIOM2001): formation, diversity, evolution and application. In: Kobayashi, Ozawa (eds) *Proceedings of the 8th int sympo biomineral*. Tokai Univ Press, Kanagawa, pp 194–201
66. Iijima M, Takita H, Moriwaki Y, Kuobki Y (1991) Difference on the organic components between the mineralized and the non-mineralized layers of lingula shell. *Comp Biochem Phys* 98A:379–382
67. Paselo M et al (2010) Nomenclature of the apatite supergroup minerals. *Eur J Mineral* 22:163–179
68. Landis WL (1999) An overview of vertebrate mineralization with emphasis on collagen-mineral interaction. *Gravit Space Bull* 12(2):15–26
69. Aoki H, Kato K, Tabata T (1977) Osteo-compatibility of apatite ceramics in mandibles, official report of the Institute for Medical Instruments. *Tokyo Med Den Univ* 11:33
70. Kuboki Y et al (1988) Remedy for a skin disease, Japanese Patent Showa 63-107938
71. Kuboki Y, Tazaki M, Mizuno M, Fujita K (1987) Mechanical filling of the micro-defects of enamel surface with HAP: the interaction between the solid surface and fine powders of the same material. *Dent J* 26(2):215–223
72. Kuboki Y et al (1989) Dental micro-investment method and its material, Japanese Patent Heisei 01-11608
73. Kuboki Y et al (2007) Development of a new purification method of active organic factors from sea shell. *Annu Sci Rep North Adv Center Sci Tech* 2007:77
74. Kuboki Y, Yagami G, Furusawa T (2017) New principles of regenerative medicine: with special reference to mechano-dynamic factors. *J Oral Tissue Eng* 14(3):128–152
75. Kuboki Y, Jin Q, Takita H (2001) Geometry of carriers controlling phenotypic expression in BMP-induced osteogenesis and chondrogenesis. *J Bone Joint Surg* 83-A:S1–S105
76. Kuboki Y, Jin Q, Kikuchi M, Mamood J, Takita H (2002) Geometry of artificial ECM: sizes of pores controlling phenotype expression in BMP-induced osteogenesis and chondrogenesis. *Connect Tissue Res* 43:529–534

77. Kuboki Y, Sasaki M, Saito A, Takita H, Kato H (1998) Regeneration of periodontal ligament and cementum by BMP-applied tissue engineering. *Eur J Oral Sci* 106(Suppl 1):197–203
78. Kuboki Y, Saito T, Murata M, Takita H, Mizuno M, Inoue M, Nagai N, Poole AR (1995) Two distinctive BMP-carriers induce zonal chondrogenesis and membranous ossification, respectively; geometrical factors of matrices for cell-differentiation. *Connect Tissue Res* 32:219–226
79. Kuboki Y, Takita H, Kobayashi D, Tsuruga E, Inoue M, Murata M, Nagai N, Dohi Y, Ohgushi H (1998) BMP-induced osteogenesis on the surface of hydroxyapatite with geometrically feasible and nonfeasible structures: topology of osteogenesis. *J Biomed Mater Res* 39:190–199
80. Itoh H, Wakisaka Y, Ohnuma Y, Kuboki Y (1994) A new porous hydroxyapatite ceramic prepared by cold isostatic pressing and sintering synthesized flaky powder. *Dent Mater J* 13: 25–35
81. Tsuruga E, Takita H, Itoh H, Wakisaka Y, Kuboki Y (1997) Pore size of porous hydroxyapatite as the cell-substratum controls BMP-induced osteogenesis. *J Biochem* 121:317–324
82. Kuboki Y, Iku S, Yoshimoto R, Kaku T, Takita H (2008) Modification of titanium surfaces based on the principles of the geometry of the artificial extracellular matrix (ECM). In: Tanaka J, Itoh S, Chen G (eds) *Surface design and modification of the biomaterials for clinical application*. Transworld Research Network, Kerala, pp 1–27
83. Kuboki Y et al (2009) Calcified honeycomb-shaped collagen maintains its geometry *in vivo* and effectively induces vasculature and osteogenesis. *Nano Biomed* 1:85–94
84. Urist MR (1965) Bone: formation by autoinduction. *Science* 150(3698):893–899
85. Reddi AH, Huggins CB (1973) Influence of geometry of transplanted tooth and bone on transformation of fibroblasts. *Proc Soc Exp Biol Med* 143:634–637
86. Ripamonti U, Crooks J, Kirkbride AN (1999) Sintered porous hydroxyapatite with intrinsic osteoinductive activity: geometric induction of bone formation. *S Afr J Sci* 95:335–343
87. Smith AH, Lingas EO, Rahman M (2000) Contamination of drinking-water by arsenic in Bangladesh: a public health emergency. *Bull World Health Organ* 78(9):1093–1103
88. Smith AH (1997) Report and action plan for arsenic in drinking water focusing on health, Bangladesh. Assignment report, WHO project BAN CWS 001, March 1997. <http://socrates.berkeley.edu/~asrg/>
89. Smith AH (1998) Technical report and review of action plan for arsenic in drinking water in Bangladesh focusing on health. Assignment Report, WHO project BAN CWS 001/D, February 1998. <http://socrates.berkeley.edu/~asrg/>
90. Smith AH (1998) Technical report. Assignment report, WHO project BAN CWS 001, June 1998. <http://socrates.berkeley.edu/~asrg/>
91. Sasaki K, Hayashi Y, Toshiyuki K, Guo (2018) Simultaneous immobilization of borate, arsenate, and silicate from geothermal water derived from mining activity by co-precipitation with hydroxyapatite. *Chemosphere* 207(9):139–146
92. Islam M, Mishra PC, Patel R (2011) Arsenate removal from aqueous solution by cellulose-carbonated hydroxyapatite nanocomposites. *J Hazard Mater* 189(3):755–763. <https://doi.org/10.1016/j.jhazmat.2011.03.051>
93. Liu G, Talley JW, Na C, Larson SL, Wolfe LG (2010) Copper doping improves hydroxyapatite sorption for arsenate in simulated groundwaters. *Environ Sci Technol* 44(4):1366–1372
94. Rouff AA, Ma N, Kustka AB (2016) Adsorption of arsenic with struvite and hydroxylapatite in phosphate-bearing solutions. *Chemosphere* 146(3):574–581
95. Katz EP, Li S-T (1973) Structure and function of bone collagen fibrils. *J Mol Biol* 80(1):1–15
96. Freundlich HMF (1906) Over the adsorption in solution. *J Phys Chem B* 57:385–470
97. Langmuir I (1918) The adsorption of gases on plane surfaces of glass, mica, and platinum. *J Am Chem Soc* 40:1361–1403
98. Langmuir I (1916) The constitution and fundamental properties of solids and liquids. Part I. Solids *J Am Chem Soc* 38:2221–2295
99. Moreno JC, Rigoberto G, Liliana G (2010) Removal of Mn, Fe, Ni and Cu ions from wastewater using cow bone charcoal. *Materials* 3:452–466

100. Meyn M, Beneke K, Lagaly G (1990) Anion-exchange reactions of layered double hydroxides. *Inorg Chem* 29:5201–5207
101. Dimotakis ED, Pinnavaia TJ (1990) New route to layered double hydroxides intercalated by organic anions: precursors to polyoxometalate-pillared derivatives. *Inorg Chem* 29:2393–2394
102. De Roy A, Forano C, El Malki K, Besse J-P (1992) Anionic clays: trends in pillaring chemistry. In: Ocelli ML, Ronson H (eds) *Expanded clays and other microporous solids. Synthesis of microporous materials*. Springer, p 108
103. Ocelli ML, Robson HE (1992) *Expanded clays and other microporous solids*. In: *Synthesis of microporous materials, vol vol II*. Van Nostrand Reinhold
104. Taylor RM (1984) The rapid formation of crystalline double hydroxy salts and other compounds by controlled hydrolysis. *Clay Miner* 19:591–603
105. Miyata S (1975) The syntheses of hydrotalcite-like compounds and their structures and physico-chemical properties-i: the systems Mg^{2+} - Al^{3+} - NO_3^- , Mg^{2+} - Al^{3+} - Cl^- , Mg^{2+} - Al^{3+} - ClO_4^- , Ni^{2+} - Al^{3+} - Cl^- and Zn^{2+} - Al^{3+} - Cl^- . *Clay Clay Miner* 23:369–375
106. Velu S, Suzuki K, Osaki T (1999) Selective production of hydrogen by partial oxidation of methanol over catalysts derived from CuZnAl-layered double hydroxides. *Catal Lett* 62:159–167
107. Bocclair JW, Baterman PS (1999) Synthesis and characterisation of layered double hydroxide dispersions in organic solvents. *Chem Mater* 11:298–302
108. Klaus Noweck B, Klaus Diblitz S, Jan Sohiefler H, Andrea Brasch M (2003) United States patent
109. Mehrotra RC (1988) Synthesis and reactions of metal alkoxides. *J Non-Cryst Solids* 100:1–15
110. Vierheilig AA (1999) US patent
111. Miyata S (1983) Anion-exchange properties of hydrotalcite-like compounds. *Clay Clay Miner* 31:305–311
112. Barriga C, Jones W, Malet P, Rives V, Ulibarri MA (1998) Synthesis and characterization of polyoxovanadate-pillared Zn-Al layered double hydroxides: an x-ray absorption and diffraction study. *Inorg Chem* 37:1812–1820
113. Ambroggi V, Fardella G, Grandolini G, Perioli L (2001) Intercalation compounds of hydrotalcite-like anionic clays with antiinflammatory agents - I. intercalation and in vitro release of ibuprofen. *Int J Pharm* 220:23–32
114. Choy JH, Park JS, Kwak SY, Jeong YJ, Han YS (2000) Layered double hydroxide as gene reservoir. *Mol Cryst Liq Cryst Sci Technol Sect A Mol Cryst Liq Cryst* 341:425–429
115. Choudary BM, Madhi S, Chowdari NS, Kantam ML, Sreedhar B (2002) Layered double hydroxide supported nanopalladium catalyst for Heck-, Suzuki-, Sonogashira-, and Stille-type coupling reactions of chloroarenes. *J Am Chem Soc* 124:14127–14136
116. Choudary BM, Kantam ML, Neeraja V, Koteswara Rao K, Figueras F, Delmote L (2001) Layered double hydroxide fluoride: a novel solid base catalyst for C-C bond formation. *Green Chem* 3:257–260
117. Motokura K, Mizugaki T, Ebitani K, Kaneda K (2004) Multifunctional catalysis of a ruthenium-grafted hydrotalcite: one-pot synthesis of quinolines from 2-aminobenzyl alcohol and various carbonyl compounds via aerobic oxidation and aldol reaction. *Tetrahedron Lett* 45:6029–6032
118. Friedrich HB, Govender M, Makhoba X, Ngcobo TD, Onani MO (2003) The Os/Cu-Al-hydrotalcite catalysed hydroxylation of alkenes. *Chem Commun* 3:2922–2923
119. Corma A, Palomares AE, Rey F, Márquez F (1997) Simultaneous catalytic removal of SOx and NOx with hydrotalcite-derived mixed oxides containing copper, and their possibilities to be used in FCC units. *J Catal* 170:140–149
120. Fearon PK, Marshall N, Billingham NC, Bigger SW (2001) Evaluation of the oxidative stability of multiextruded polypropylene as assessed by physicochemical testing and simultaneous differential scanning calorimetry-chemiluminescence. *J Appl Polym Sci* 79:733–741
121. Leroux F, Besse J (2001) Polymer interleaved layered double hydroxide: a new emerging class of nanocomposites. *Chem Mater* 13:3507–3515

122. Benotti MJ, Trenholm RA, Vanderford BJ, Holady JC, Stanford BD, Snyder SA (2009) Pharmaceuticals and endocrine disrupting compounds in U.S. drinking water. *Environ Sci Technol* 43:597–603
123. Maichin F, Freitas LC, Ortiz N (2013) The use of converter slag (magnetite) and bentonite clay for amoxicillin adsorption from polluted water, orbital electron. *J Chem* 5:1–5
124. Abdolmohammad-Zadeh H, Kohansal S, Sadeghi GH (2011) Nickel-aluminum layered double hydroxide as a nanosorbent for selective solid-phase extraction and spectrofluorometric determination of salicylic acid in pharmaceutical and biological samples. *Talanta* 84:368–373
125. Abdolmohammad-Zadeh H, Kohansal S (2012) Determination of mesalamine by spectrofluorometry in human serum after solid-phase extraction with Ni-Al layered double hydroxide as a nanosorbent. *J Braz Chem Soc* 23:473–481
126. Khatem R, Miguel RO, Bakhti A (2015) Use of synthetic clay for removal of diclofenac anti-inflammatory. *Eurasian J Soil Sci* 4:126
127. Dwiasi DW, Mudasir M, Roto R (2020) Solid-phase extraction of amoxicillin in aqueous system by using Mg-Al-oxalate ldh as a stationary phase. *Rasayan J Chem* 13:2523–2529